Nucleoside Diphosphate Kinase-3 (*NME3*) Enhances TLR5-Induced NF-κB Activation

Kelly Flentie[1,*], Caleb Gonzalez[2,*], Brandon Kocher[1], Yue Wang[3], Hongtu Zhu[3], Jayne Marasa[1], David Piwnica-Worms[2,4]

[1]Mallinckrodt Institute of Radiology, Washington University School of Medicine, St. Louis, MO 63110

[2]Department of Cancer Systems Imaging, [3]Department of Biostatistics, University of Texas M.D. Anderson Cancer Center, Houston, TX 77030

Keywords: NME3, cancer, TLR5, screen, luciferase, reporter, flagellin, *Salmonella*, NF-κB

No COI declared.

Running Title: TLR5-Induced NF-κB Activation is Enhanced by *NME3*

Financial Support: UT STARs Award, P50 CA94056, P30 CA91842 and P30 CA016672.

***Co-first authors**

[4]Corresponding author:
David Piwnica-Worms, M.D., Ph.D.,
Department of Cancer Systems Imaging,
The University of Texas M.D. Anderson Cancer Center,
1400 Pressler Street, Unit 1479
FCT16.6030, Houston, Texas 77030
Tel: 713-745-0850
Fax: 713-745-7540
Email: dpiwnica-worms@mdanderson.org

Abstract

Bacterial flagellin is a potent activator of NF-κB signaling, inflammation and host innate immunity, and recent data indicate that flagellin represents a novel anti-tumor ligand acting through toll-like receptor 5 (TLR5) and the NF-κB pathway to induce host immunity and aid in the clearance of tumor xenografts. To identify innate signaling components of TLR5 responsible for these anti-tumor effects, a loss-of-function high-throughput screen was employed utilizing carcinoma cells expressing a dynamic NF-κB bioluminescent reporter stimulated by *Salmonella typhimurium* expressing flagellin. A live cell screen of a siRNA library targeting 691 known and predicted human kinases to identify novel tumor cell modulators of TLR5-induced NF-κB activation uncovered several interesting positive and negative candidate regulators not previously recognized, including nucleoside diphosphate kinase 3 (NME3), characterized as an enhancer of signaling responses to flagellin. Targeted knockdown and overexpression assays confirmed the regulatory contribution of NME3 to TLR5-mediated NF-κB signaling, mechanistically downstream of MyD88. Furthermore, Kaplan-Meier survival analysis showed that NME3 expression correlated highly with TLR5 expression in breast, lung, ovarian, and gastric cancers, and furthermore, high-level expression of NME3 increased overall survival for patients with breast, lung and ovarian cancer, but the opposite in gastric cancer. Together, these data identify a previously unrecognized pro-inflammatory role for NME3 in signaling downstream of TLR5 that may potentiate cancer immunotherapies.

Implications

Pro-inflammatory signaling mediated by innate immunity engagement of flagellin-activated TLR5 in tumor cells results in anti-tumor effects through NME3 kinase, a positive downstream regulator of flagellin-mediated NF-κB signaling, enhancing survival for several human cancers.

Introduction

Harnessing host immunity constitutes a promising cancer therapeutic strategy (1-3), and agonists of Toll-like receptors (TLRs) have been actively pursued for their antitumor potential, either as monotherapy or as adjuvants to vaccination or other therapeutic modalities (4-6). In this context, *Salmonella typhimurium*, a common flagellated facultative intracellular bacterial pathogen, has been identified as a potential tumor therapeutic, capable of inducing tumor regression (7-13). While the exact mechanisms behind *Salmonella* therapeutic efficacy remain unclear, the effects are thought to be mediated by bacterial antigenicity and activation of host innate immune responses mediated by the TLR family of pattern recognition receptors (14,15). Several groups have shown that mouse tumor xenografts are uniquely sensitive to treatment with bacterial flagellin, resulting in tumor regression (16-19), likely mediated by TLR5, which specifically binds flagellin (20). The induced pro-inflammatory signals appear to reside within the cancer cells *per se* since cancer cells lacking TLR5 fail to respond to treatment with flagellin *in vivo* (16).

TLR5 is an important conventional component of innate immunity and interesting, also may be involved in maintaining genomic stability through its integration into the DNA-damage p53 regulatory network (21). The enhancement of TLR5-mediated recruitment of the innate immune response by p53 points towards an important crossroad between cancer progression and treatment (22,23). TLR5 acts by recognizing flagellated bacteria, such as *Salmonella,* alerting the host of their presence (24,25). Once bound by activating ligand, TLR5 initiates a signaling cascade that ultimately impacts transcription in host cells resulting in activation of pro-inflammatory pathways, which include NF-κB (16,24). To initiate NF-κB signaling, activated TLR5 induces recruitment of the cytosolic adapter, MyD88, which interacts directly with the

Toll-interleukin-1 receptor (TIR) domain (24). MyD88 then recruits the serine/threonine kinase IRAK (IL-1 receptor-associated kinase), and via phosphorylation, IRAK activates TNFα-receptor-associated factor (TRAF6), which in turn activates TRAF-associated kinase (TAK) (26). TAK links TRAF6 to the IKK complex, which phosphorylates IκBα, the negative regulator of NF-κB (24). Canonical ubiquitination and proteasome-mediated degradation of IκBα frees NF-κB to translocate into the nucleus and activate downstream transcriptional programs that promote inflammation and immune responses (24). This robust activation of host innate immunity signaling has been postulated to mediate chemokine secretion and tumor regression (16).

In NF-κB signaling, various induction signals, inclusive of, but not limited to, pathogen-associated ligands, reactive oxygen species, cytokines and DNA damage, lead to activation of transcriptional programming specifically designed to shape responses to each cellular stress (27). As multiple different triggers are capable of inducing NF-κB, multiple cellular outcomes exist in response to each insult (27,28). To further complicate the scenario, the resulting transcriptional profile and downstream effects of NF-κB signaling may differ based on specific cell contexts (29). For example, a beneficial pro-inflammatory signal in an acute exposure may transition to a tumorigenic signal in a chronic context. Indeed, acute activation of NF-κB in an individual tumor cell may activate host defenses to isolate transformed cells, but in T cells, flagellin has been shown to upregulate PD-1 expression, an immune checkpoint receptor, which may enable tumor cells to escape immune surveillance (30). Interestingly, interactions between commensal microbiota in the gut and TLR5 have been recently reported to modulate systemic inflammatory responses that may suppress or accelerate distal cancers depending on context (31).

Using a bioluminescence reporter, we herein confirmed a robust activation of pro-inflammatory TLR5-mediated NF-kB signaling in HCT116 human colon carcinoma cells by bacterial flagellin. Then, to identify novel regulatory components of innate immunity and TLR5 signaling that may contribute to the pro-inflammatory signals mediating the anti-tumor effects of flagellin, we employed a high throughput siRNA screen. After assessing the contribution of 691 human kinases, we identified a nucleoside diphosphate kinase**,** NME3, as a positive regulator of NF-κB signaling in response to flagellin. Expression of this kinase, which we demonstrate to be required for maximal TLR5 signaling by bacterial flagellin, is also correlated with enhanced survival rates in lung, breast and ovarian cancer patients. In addition to NME3, this investigation also identified multiple candidates that may serve as adjuvant targets to support the anti-tumor properties of flagellin.

Materials and Methods

Cell lines and culture conditions

HCT116 human colon carcinoma cells (TP53 WT) were a gift of Bert Vogelstein (2009) and cultured according to ATCC instructions (11). Mycoplasma testing was performed routinely. Further cell line authentication was not performed. All stably transfected HCT116 cells were cultured in 0.5 µg/ml puromycin.

Salmonella strains

Salmonella typhimurium strain SL1344 was used for all experiments, except where noted. All mutants (*fliC*$^{-}$, *fljB*$^{-}$ and *fliC*$^{-}$*fljB*$^{-}$) were constructed using a lambda red recombinase strategy (32). First, primers were designed to amplify the kanamycin- or chloramphenicol-resistance cassette in *pKD4* or *pKD3* with tails flanking the targeted locus of the *Salmonella* genome to be

deleted. PCR fragments were then electroporated into SL1344 bacteria expressing plasmid-encoded red recombinase. Following electroporation, growth on kanamycin or chloramphenicol plates at 37°C selected for strains that had lost the temperature-sensitive recombinase plasmid and inserted the chloramphenicol-resistance cassette into the targeted genomic locus. The double mutant strain was created in a step wise manner, by individually deleting each gene. Deletion of target genes was confirmed by PCR.

Creation of a κB$_5$:IκBα-FLuc*-expressing HCT116 stable cell line*

HCT116 cells at 95% confluency were co-transfected with 10 µg of *pκB$_5$:IκBα-FLuc* and 3 µg of *pIRES-puro* plasmid DNA using Fugene 6 (Roche) in 10 cm dishes (33). After 24 hours, the media was replaced with fresh cell media. Twenty-four hours later, the cells were split at multiple dilutions into media containing 0.5 µg/ml puromycin to select for stable transformants. After two weeks, isolated cell colonies were imaged to confirm reporter gene expression and bioluminescent colonies were harvested and expanded. Reporter cells were continuously cultured in the presence of 0.5 µg/ml puromycin to maintain expression of the reporter plasmid.

Transient transfections of HCT116 cells

HCT116 cells were transiently transfected where noted. Cells were plated in 24-well (50,000-60,000 cells/well) or 96-well (10,000 cells/well) plates and transfected with Fugene 6 and 200 ng of plasmid DNA (24-well) or 50 ng of plasmid DNA (96-well) per well. In the case of NME3 over-expression experiments, reporter cells were transfected with Fugene 6 and 100 ng of target (*pCMV6:NME3*) or vector control (*pCMV6*) plasmid in each well of a 96-well plate. Alternatively, 100 ng of reporter plasmid and 200 ng of target (*pCMV6:NME3*) or vector control

(*pCMV6*) plasmid were used in each well of a 24-well plate. Cells were allowed to recover for 48 hours prior to imaging.

Dynamic imaging of NF-κB signaling

Thirty minutes prior to imaging, cell media were aspirated and replaced with colorless DMEM or McCoy 5A supplemented with 10% heat-inactivated FBS and 150 µg/ml *d*-luciferin. Cells were imaged at baseline and after stimulation as indicated in an IVIS 100 or IVIS 50 imaging system, with images being acquired every 5 minutes for 6 hours, unless otherwise indicated. Cells were maintained in the imaging chamber by a heated stage (37ºC) and 5% CO_2 air flow. Acquisition parameters were: acquisition time, 60 sec; binning, 4-8; filter, open; f stop, 1; FOV, 12-23 cm. Stimuli included: SL1344 *Salmonella typhimurium*, or indicated mutants, processed from confluent culture (final dilution 1:100 in well) or SL1344 matched for OD_{600}, heat-killed by boiling 10 minutes and diluted 1:10, 1:100 or 1:1000 into each well (where noted); lipopolysaccharide (1 µg/ml) (Sigma); peptidoglycan (Sigma); iEDAP (10 µg/ml) (InvivoGen); MDP (10 µg/ml) (InvivoGen); TNFα (20 ng/ml) (R & D systems); flagellin (InvivoGen); anti-hTLR5-IgA (10 µg/ml) (InvivoGen); or shTLR5-FC (5 µg/ml) (InvivoGen). Bioluminescence photon flux (photons/sec) data represent the mean of triplicate wells for the indicated number of independent experiments, and were analyzed by region of interest (ROI) measurements with Living Image 3.2 (Caliper Life Sciences). Data were imported into Excel (Microsoft Corp.), averaged, and normalized to both initial (t = 0) values (fold-initial) and vehicle-treated controls (fold-vehicle) for presentation in dynamic plots (34).

High-throughput screen

Author Manuscript Published OnlineFirst on March 9, 2018; DOI: 10.1158/1541-7786.MCR-17-0603
Author manuscripts have been peer reviewed and accepted for publication but have not yet been edited.

siRNA screening in triplicate was performed in white, clear-bottomed, 96-well culture plates using a Beckman-Coulter Core Robotics system, including an FX liquid handler, controlled by the Sagian graphical method development tool (SAMI scheduling software). HCT116 cells stably expressing *pκB$_5$:IκBαFLuc* were seeded at 15,000 cells per well in a 96 well plate and cells were allowed to attach for 24 hours. Forward transfection was performed with a 96 multichannel head on the FX liquid handler, adding 0.5 µl/well of media-complexed R1 Transpass (NEB) to the aliquotted siRNA library (Kinase siRNA set v2; Qiagen Inc.) in a 96-well reaction plate and allowed to incubate for 15 minutes. After incubation of siRNA complexes, 100 µl was added to each well of a plate with cells (x3 plates) using the FX liquid handler, yielding a final concentration of ~50 nM siRNA/well. Experimental siRNA oligos were arrayed in columns 2-11 of each plate and individual controls comprising vehicle-treated wells, a non-targeting control sequence (Qiagen Allstar Negative control), *TLR5*-targeting siRNA sequences (IDT), and a firefly luciferase-targeting *PGL3* siRNA (Dharmacon Research Inc.) were placed manually in columns 1 and 12. Plates were maintained at 37ºC and 5% CO_2 for 48 hrs. At this time, media were aspirated and replaced with 180 µl imaging media (colorless DMEM supplemented with 10% heat inactivated FBS and 150 µg/ml *d*-luciferin) and the cells were allowed to equilibrate for 45 minutes. After equilibrating, 20 µl of stimulus (1:100 dilutions of heat-killed *Salmonella* cultures) or control (LB broth) were added to each well. Bioluminescent readings were obtained on an EnVision plate reader (PerkinElmer) immediately following the stimulus, at 45 minutes post-stimulation and at 245 minutes post-stimulation. After the final luminescent reading, 20 µl of rezasurin dye was added to all wells, allowed to incubate for 2 hours at 37^{0}C and monitored on a FLUOstar OPTIMA fluorescence reader for cell viability (BMG Labtech; excitation, 544 nm; emission, 590 nm).

Data analysis

Initially, signal in each well was normalized to a plate-matched control well containing a non-targeting siRNA sequence at each time point to facilitate experiment-wide analysis. Then, the differences in the $\log_2$ values of the normalized data between 0 minutes and 45 or 245 minutes were averaged across triplicate siRNA experimental replicates. Then, screening hits were selected by quartile analysis of the normalized kinase library data. To perform the quartile analysis, median (Q2), first (Q1) and third (Q3) quartile values were calculated. From these values, the upper and lower boundaries for hit selection were calculated as Q3 + 2c(Q3 –Q2) and Q1 – 2c(Q2-Q1), respectively, for c = 1.2245 corresponding to a high-stringency targeted error rate (α =0.02) and for c = 0.7193 corresponding to a low-stringency targeted error rate (α = 0.1) (35).

siRNA knockdown validation

Knockdown of *NME3* or *MyD88* was performed utilizing heterogeneous mixtures of siRNAs targeting *NME3* or *MyD88* mRNA sequence, respectively. Reporter HCT116 cells were plated in 96-well plates at 15,000 cells/well and allowed to incubate overnight. Twenty-four hours later, cells were transfected with X-tremeGene siRNA transfection reagent (Sigma) and 25 nM esiRNA (Sigma). Cells were incubated in media for 72 hours prior to imaging. Additional siRNA knockdown of *NME3* was performed utilizing 4 separate targeting sequences. Reporter HCT116 cells were treated as before with the exception that cells were transfected with R1 Transpass (NEB) and 25 nM siRNA (Qiagen) as per R1 Transpass instructions. Cells were incubated in media for 72 hours prior to imaging.

shRNA lentiviral knockdown cell line construction

Lentivirus-expressing constructs (*pLKO.1 puro*) were obtained pre-synthesized from the Genome Institute at Washington University. The targeting sequences for the 3 *shNME3* constructs are as follows:

#7 - 5' GAGGTTGGCAAGAACCTGATT

#8 - 5' GCCTTGTCAAGTATATGGCCT

#9 - 5'CGAGAGGAAGGGCTTCAAGTT

Additionally, a scrambled *shRNA* construct was utilized as a negative control. To generate lentivirus containing hairpins, 293T cells ($5x10^5$) were pre-plated in 60 mm dishes and co-transfected the following day with 1 µg of hairpin construct, 900 ng packaging plasmid p*CMV:ΔR8.2*, and 100 ng of envelope plasmid p*VSVG* using Fugene 6. Two days after transfection, virus-containing supernatant was collected from 293T cells and filtered through a 0.45 µm filter, mixed with 5 µg/ml protamine sulfate, and added to HepG2 cells at 50% confluency in a 10 cm^2 dish. Media was replenished 12 hrs post-transduction, and cells were subsequently maintained in media supplemented with 500 ng/ml puromycin hydrochloride to retain expression of the hairpins. Following transduction, *shNME3* or *shSCRAMBLED* cells were plated in parallel for mRNA knockdown confirmation and transient transfection and subsequent imaging measurements with the *κB$_5$:IκBα-FLuc* reporter or the *κB$_5$:FLuc* reporter as described.

Semi-quantitative RT-PCR

HCT116 cells transfected with siRNA targeting either *NME3* or *MyD88* were lysed and total RNA was purified using the Qiagen RNeasy kit (Qiagen). cDNA synthesis was performed using iScript Advanced cDNA Synthesis Kit for RT-qPCR (Bio-Rad) using 800 ng of total RNA per reaction. To perform quantitative PCR, 100 ng of cDNA per sample were amplified with primer

specific for either human *NME3* or human *MyD88* (PrimePCR SYBR Green, Bio-Rad) using SsoAdvanced Universal SYBR Green Supermix (Bio-Rad). PCR cycling conditions were: 95°C for 30 seconds for polymerase activation and DNA denaturation, followed by 42 cycles of denaturalization (95°C for 10 seconds) and annealing/extension/plate read (60°C for 30 seconds).

HCT116 cells transduced with *shNME3* or *shSCRAMBLED* hairpins were lysed and total RNA was purified using the Qiagen RNeasy kit (Qiagen). Samples were then treated with DNase I at room temperature for 15 minutes, after which EDTA was added and samples were incubated for 10 minutes at 65°C to inactivate the DNase. Samples were then ethanol precipitated and resuspended in water. For reverse transcriptase PCR, 1 μg of total RNA was used as a template and reverse transcribed using Superscript II Reverse Transcriptase and 300 ng random primers as per the manufacturer's instructions (Invitrogen). To perform semi-quantitative PCR, samples were amplified using 2 μL of RT reaction and primers specific to *NME3* or *GAPDH*. PCR cycling conditions were: 95°C for 5 minutes, 35 cycles (or 25 cycles for *GAPDH* reactions) of denaturation at 95°C for 45 seconds, annealing at 55°C for 45 seconds and extension at 72°C for 1 minute. PCR products were fractionated on a 1% agarose gel.

Survival analysis

The univariate Cox proportional hazard model was used to assess the correlation of gene expression with patient overall survival, and the likelihood ratio test *p*-values were reported. Datasets from TCGA, GEO and caBIG (36-38) were used for determining overall survival of patients with breast cancer, lung cancer, ovarian cancer, and gastric cancer. Gehan-Breslow-Wilcoxon and Log-rank tests were used to estimate *p*-values between high and low expression groups (using top and bottom 25% as the cutoff for grouping). Chi-square tests were used to test

the association between two gene expression profiles with high (>75%), median (<75% - >25%) and low (<25%) expression levels for the entire cohort of each cancer type (39). A two-tailed $p < .05$ was considered significant. Analyses were performed using R 3.2.3.

Results

To assess TLR5-induced activation of NF-κB by *Salmonella* in real time in living cells, we utilized a bioluminescent transcriptionally coupled *κB$_5$:IκBα-FLuc* fusion reporter, consisting of the negative regulator of NF-κB, IκBα, directly fused to firefly luciferase. In this case, baseline activity of the fusion reporter protein serves as a direct readout of basal IKKβ kinase activity in the host cell (33). As activated IKKβ phosphorylates endogenous IκBα, the reporter fusion protein is similarly phosphorylated, ubiquitinated, and targeted for degradation, resulting in a reduction in bioluminescent reporter activity, which can be monitored in real time (33). Liberation of endogenous NF-κB from its inhibitor allows translocation to the nucleus and transcriptional activation of NF-κB response elements. Because the reporter construct is linked on its 5' end to five of these response elements in tandem, NF-κB nuclear transactivation drives transcription/translation of new fusion proteins resulting in an increase in bioluminescent signal (33). Thus, stimulation of HCT116 cells with heat-killed *Salmonella* robustly initiated degradation and the subsequent resynthesis of the IκBα-FLuc reporter fusion, which could be imaged periodically to visualize changes in reporter photon output (Fig. 1a) and represented graphically (Fig. 1b). Heat-killed bacteria were preferred as a stimulus over live bacteria. When performing the assay with live *Salmonella*, replication and overgrowth of the bacteria quickly changed media conditions, ultimately leading to complete attenuation of the luciferase signal.

After stimulation with heat-killed *Salmonella*, the reporter signal initially decreased to 60% of its steady state level prior to activation. Following this decrease, which corresponded to IκBα degradation, *Salmonella*-induced reporter activity rebounded to >3X the original bioluminescence levels, corresponding to transcriptional activation and translation of the IκBα-FLuc fusion protein.

Reporter Responsiveness to Flagellin-Mediated Activation of TLR5.

To isolate the specific moiety of the bacteria that activated NF-κB signaling in HCT116 carcinoma cells, we tested individual activities of known immunostimulatory components of bacteria. In HCT116 cells stably expressing the *κB$_5$:IκBα-FLuc* reporter, bacterial LPS, purified peptidoglycan (PG), and NOD ligands (MDP and iEDAP) were all incapable of inducing significant bioluminescent reporter activity (Fig. 1c-e). To determine the contribution of the two *Salmonella* flagellin proteins to NF-κB pathway activation in HCT116 cells, we constructed *Salmonella* strains mutated singly or in both flagellin genes *fliC* and *fljB*. Both single mutants still activated NF-κB signaling, albeit to a lesser extent than that of wild type bacteria, but the *Salmonella fliC$^-$/fljB$^-$* double mutant was incapable of activating NF-κB signaling (Fig. 1f), indicating that flagellin was the predominant ligand inducing NF-κB signaling in HCT116 cells.

Flagellin is the principal component of bacterial flagella, a major virulence factor recognized by mammalian TLR5 receptors (20), which upon binding activates NF-kB in a MyD88-dependent manner (40). To further define flagellin-mediated activation of the TLR5 pathway in HCT116 cells, we utilized two different bioluminescent reporters to visualize signaling in real time. First, cells containing the transcriptionally-coupled *κB$_5$:IκBα-FLuc* fusion reporter were treated with increasing concentrations of *Salmonella typhimurium*-derived flagellin (10, 20, 50, 100, 200, and

1000 ng/ml), which induced progressive increases in reporter degradation kinetics as well as transcriptional responses (Fig. 2a). Both maximal reporter degradation and resynthesis showed different kinetics compared to stimulation with TNFα, inferring differences in the signal transduction mechanism induced by the different stimuli. Similarly, concentration-dependent responses were observed when cells were treated with heat-killed *Salmonella* (Fig. 2b). To support these findings, a standard transcriptionally-activated *κB$_5$:FLuc* reporter was utilized as our second bioluminescent reporter in HCT116 cells. A concentration-dependent activation of the *κB$_5$:FLuc* reporter was confirmed when cells were treated with increasing concentrations of flagellin (5, 10, 20, 50, 100, 200 ng/mL) (Fig. S1a, b), and by heat-killed *Salmonella* (Fig. S1c, d).

Next, we confirmed that activation of the *κB$_5$:IκBα-FLuc* fusion reporter in HCT116 cells was mediated by flagellin binding to TLR5 receptors. First, we pre-incubated flagellin (at two concentrations: 100 ng/ml and 1 μg/ml) with 5 μg/ml of soluble human TLR5 (shTLR5) (molar ratios 1:27 and 1:3) for 30 min prior to addition of the activation mixture to cells. Pre-incubation of flagellin with shTLR5 abrogated flagellin-induced activation of the *κB$_5$:IκBα-FLuc* fusion reporter at both concentrations (Fig. 2c). Reporter activation could be competitively rescued by pre-incubation with a 10X increase in flagellin concentration (10 μg/ml) in the presence of the same concentration of shTLR5 (Fig. S2). As expected, pre-incubation of shTLR5 with TNFα had no significant effect on TNFα-induced activation of the *κB$_5$:IκBα-FLuc* fusion reporter (Fig. 2c). These data confirmed the specificity of the flagellin-mediated activation of the *κB$_5$:IκBα-FLuc* fusion reporter through TLR5 receptor binding. Second, we tested if an antibody directed against the extracellular domain of TLR5 (hTLR5 Ab) also inhibited flagellin-mediated activation of the *κB$_5$:IκBα-FLuc* fusion reporter. Cells were pre-incubated for 1 hour with hTLR5 Ab (10 μg/ml)

followed by treatment with flagellin at two concentrations that readily activated the reporter under standard conditions (100 ng/ml or 10 μg/ml). At the low flagellin concentration (100 ng/ml), hTLR5 Ab pre-incubation completely blocked degradation or activation of the reporter, while at the high flagellin concentration (10 μg/ml), the overall blockade was less, but the activation phase was still reduced by 2.5-fold at 6 hours (Fig. 2d). Conversely, while cells pre-incubated with hTLR5 Ab and then activated with TNFα (20 ng/ml) showed a shallower and extended degradation phase of IκBα compared with cells treated only with TNFα (20 ng/ml), consistent with cross-talk between the two pathways converging on IκBα, the transcriptional activation response was unaffected at 6 hours (Fig. 2d).

Live Cell *siRNA* Library Screen.

With the knowledge that HCT116 colon carcinoma cells were robustly activating pro-inflammatory signaling in response to *Salmonella* flagellin, we set out to identify novel cancer cell kinases regulating TLR5-mediated innate immune responses. We utilized a *siRNA* library to knockdown all known and predicted human kinases and screen for involvement of each in *Salmonella*-induced activation of the TLR5 pathway. The screen utilized HCT116 cells colon carcinoma cells stably expressing the *κB_5:IκBα-FLuc* construct. Cells were plated and transfected with *siRNA* targeting 691 host kinases arrayed in the 10 center columns of 96-well plates with each well containing two sequences targeting a single host kinase. Forty-eight hours following *siRNA* transfection, cells were stimulated with heat-killed *Salmonella* and the reporter signal was measured immediately (baseline), at 45 minutes and at 245 minutes following exposure to *Salmonella* (Fig. 3a,b). Normalized bioluminescence data at 45 and 245 minutes were plotted individually (Fig. 3c,d and Fig. S3a,b), or on x,y-coordinates representing the normalized signals at 45 and 245 minutes, respectively (Fig. 4).

High-throughput screening hits were determined using a quartile-based analysis. Figures 3 and 4 display the quartile-identified values for low- and high-stringency hit selection. *siRNA*-induced loss-of-function of cellular kinases that positively affect TLR5 signaling will demonstrate reduced responsiveness to *Salmonella*. In contrast, wells with *siRNA* targeting a negative regulator of TLR5-induced NF-κB signaling will show enhanced reporter response. Figure 4 demonstrates the four possible effects kinases in the screen may have had on reporter activity (insert). Kinase knockdowns further enhancing the loss of photon flux signal at 45 minutes, i.e., increasing IκBα degradation, indicated that a negative regulator of early TLR5-induced NF-κB signaling had been targeted. Meanwhile, kinase knockdowns attenuating the early degradation phase of signal at 45 minutes indicated that *siRNA* targeted a positive regulator of early TLR5-induced NF-κB signaling. Conversely, at the 245 minute time point, decreased values represented a low signal during the resynthesis phase, which indicated a lack of full NF-κB transactivation and therefore *siRNA* knockdown of a positive regulator of NF-κB-induced transcription. Greater photon flux values corresponded to over-activation of NF-κB transcriptional activity, and therefore *siRNA* treatment targeted a negative transcriptional regulator. Therefore, in Figure 4, a *siRNA* that targets a positive regulator of both the degradation and resynthesis phases will fall in the lower right quadrant, while a negative regulator of both phases will be found in the upper left portion of the scatter plot. The positive control well containing *siRNA* targeting TLR5, for example, should prevent IκBα degradation at 45 minutes, which in turn, will inhibit reporter transcriptional activation at 245 minutes. This is shown by the blue triangle corresponding to TLR5 *siRNA*-treated wells, which falls in the lower right quadrant of the scatter plot. Table 1 lists the top ten positive and negative regulators from each phase of the screen. Additionally, Supplementary Table 1 details all of the low- and high-stringency hits

from the screen. Of note, IRAK1 and AKT1, both known activators of NF-κB signaling, were identified as hits in the screen, further verifying the validity of the strategy. The screen also identified MAP2K2, MAP2K3, and PIK3CG, PIK3CD, among others, as kinases involved in positively regulating flagellin-induced NF-κB signaling. However, targeting known downstream MAP kinases with chemical inhibitors (U0126, SB203580) showed no consistent effect in this system, and given this complexity, MAP kinase pathways were not further pursued. Notably, CDK6, a known anticancer drug target (41), CDK5R2, and TYRO3 were affirmed as negative regulators of TLR5-induced NF-κB signaling.

Interestingly, one of the novel hits identified in the screen was NME3, a nucleoside diphosphate kinase that catalyzes the formation of other nucleoside triphosphates from ATP. NME3 was originally named based on the discovery of the gene by preferential expression in **n**on-**me**tastatic (nme) cells in a cancer model and has subsequently been demonstrated to possess anti-cancer properties in multiple model systems upon over-expression (42-45). In the screen, knockdown of *NME3* attenuated reporter signal at 45 minutes and caused reduced TLR5-induced transcriptional activation at 245 minutes, indicating that NME3 was behaving as both a positive regulator of degradation and transcription of NF-κB signaling (Fig. 4).

Given that MyD88 is an essential signal adaptor of TLR5-mediated activation of NF-kB signaling (46), we first confirmed the signature of *MyD88 siRNA* knockdown on *Salmonella*-stimulated activation of the *κB_5:IκBα-FLuc* fusion reporter in this system. Figure 5a shows that knockdown of *MyD88* by *siRNA* markedly reduced both the degradation and resynthesis phases of NF-κB signaling compared to scrambled control. The signal showed virtual, but not complete abrogation, likely due to incomplete knockdown of *MyD88* (Fig. 5a, bottom right). Overall, these results further affirmed that activation of the *κB_5:IκBα-FLuc* fusion reporter by flagellin was

mediated through TLR5. Then, we confirmed that knockdown of *NME3* by pooled heterogeneous *siRNA* sequences (Fig. 5a) and four individual *siRNA* sequences (Fig. S4a) recapitulated data in the primary screen. Of note, the kinetics of degradation were blunted, but not blocked (as was observed upon knockdown of MyD88), placing NME3 downstream of MyD88. Quantitative PCR confirmed that *NME3 mRNA* levels were indeed reduced in cells treated with pooled *NME3 siRNA* sequences compared to cells treated with scramble *siRNA* sequence (Fig. 5a, top insert). Semi-quantitative analysis of cell viability showed no significant effect on cell growth/survival in *NME3* knockdown compared with scrambled *siRNA* controls.

To further determine the contribution of NME3 to TLR5-induced activation of NF-κB, we produced stable knockdown of *NME3* in HCT116 cells using lentiviral shRNA constructs. Knockdown of *NME3* by shRNA in wildtype HCT116 cells did indeed interfere with TLR5 signaling (Fig. 5b). Compared to cells expressing a scrambled shRNA sequence, cells expressing *shRNA* targeted to *NME3* again showed less reporter degradation, slower kinetics, and substantially less resynthesis of the reporter during the transcriptional activation phase. The responsiveness of a purely transcriptional reporter was also tested in HCT116 cells. As was seen with *NME3*-knockdown cells expressing the *κB_5:IκBαFLuc* reporter, cells expressing a *κB_5:FLuc* construct also showed considerably less TLR5-driven transcriptional activation following *Salmonella* stimulation (Fig. 5c). Semi-quantitative PCR confirmed that *NME3* mRNA in targeted shRNA-expressing cells was indeed reduced to low levels compared to cells containing a non-targeting shRNA construct (Fig. 5d).

Conversely, to test whether over-expression of NME3 potentiated TLR5-induced NF-κB signaling, we over-expressed plasmid-encoded *NME3* in HCT116 cells expressing the *κB_5:IκBα-FLuc* reporter. Over-expression of NME3 induced higher levels of *Salmonella*-stimulated

transcriptional activation, further demonstrating that NME3 was a positive regulator of TLR5-induced NF-κB signaling (Fig. 5e and Fig. S4b).

Survival Analysis.

NF-κB signaling is well known to have both tumor promoting and tumor suppressive roles through cell autonomous, innate pro-inflammatory signaling (47-49). Having identified NME3, which has previously been shown to have tumor suppressor-like functions (43,45,50), as a novel enhancer of TLR5-induced NF-κB activation, we hypothesized that NME3 may participate in tumor suppression through positive activation of this pro-inflammatory signaling pathway. To begin to explore the clinical relevance of this proposed mechanism, we utilized cancer patient clinical expression profiles and mutational analysis tools. Kaplan-Meier survival analysis for breast (n = 3,951; Relapse Free Survival) (36) and lung (n = 1926; Overall Survival) (37) cancer patients showed that patients with high level expression of *NME3* correlated with increased survival compared to patients with low levels of *NME3* ($p < 0.0001$ and $p < 0.0001$) **(**Fig. 6, a-b). For ovarian cancer, median survival increased with higher expression of *NME3*, but long term survival did not; overall survival differences were not significant (n = 1435; Progression Free Survival) ($p < 0.22$) (38) **(**Fig. 6c). In contrast, gastric cancer patients (n=876) with higher *NME3* expression showed decreased overall survival ($p < 0.002$) (Fig. 6d).

Consistent with our hypothesis, *TLR5* clinical survival analysis correlated with *NME3* survival analysis. Breast (n = 3,951; Relapse Free Survival) (36), lung (n = 1926; Overall Survival) (37), and ovarian (n = 1435; Progression Free Survival) (38) cancer patients with higher *TLR5* expression levels showed enhanced survival ($p < 0.0001$, $p < 0.0001$ and $p < 0.01$, respectively) **(**Fig. S5, a-c**)**, whereas gastric cancer patients (n=876; Overall Survival) with higher *TLR5*

expression levels showed decreased survival ($p < 0.02$) (Fig. S5d). Indeed, overall *TLR5* expression profiles significantly associated with *NME3* expression profiles for breast (n=3951), lung (n=1926), ovarian (n=1435), and gastric (n=876) cancer patients (Pearson residual) (Fig. 7 a-d). Of interest, higher expression of *NF-κB1* (*p50*) only correlated with better survival for breast cancer (n = 3,951; Relapse Free Survival) ($p < 0.0001$) (Fig. S6a), but not for lung (n = 1926; Overall Survival) (37), ovarian (n = 1435; Progression Free Survival) or gastric cancer (n=876; Overall Survival) ($p < 0.11$, $p < 0.27$ and $p < 0.22$, respectively) (Fig. S6, b-d). However, low, median and high *NF-κB1* expression was significantly associated with *NME3* and *TLR5* expression profiles of breast (n=3951, $p <0.0001$, and n=3951, $p < 0.0001$, respectively), lung (n=1926, $p < 0.0001$, and n=1926, $p < 0.0001$), ovarian (n=1435, $p < 0.0001$, and n=1435, $p < 0.0001$), and gastric (n=876, $p < 0.008$, and n=876, $p < 0.0001$) cancer patients.

Discussion

Salmonella engagement of TLR5 and activation of NF-κB serves primarily to alert the host of invading pathogens, which is accomplished by activating specific signaling pathways, release of cytokines and recruitment of host immune cells to the local microenvironment. Agonists of TLRs have been actively pursued for their antitumor potential, and in this context, co-opting evolutionarily conserved pathways for tumor colonization by *Salmonella* has been explored due to the capacity of the bacterium to specifically localize to tumors *in vivo* with minimal host side-effects (7,8,10). Furthermore, recent studies have shown that *Salmonella* flagellin provides potent anti-tumor effects capable of suppressing tumor growth (7-13). Taken together, these data provide a basis for development of a *Salmonella*-based treatment strategy taking advantage of TLR5-mediated activation of NF-κB following tumor-specific flagellin delivery.

Herein, using HCT116 colon carcinoma cells, we demonstrated that stimulation of TLR5 with flagellated *Salmonella* robustly activated pro-inflammatory NF-κB signaling in a tumor cell-autonomous manner, and that the bacterial flagellin, and not other known immunostimulatory moieties, was necessary for this pro-inflammatory signaling event. Note that our results stand in contrast with another study (15) that reported that stimulation *in vitro* with bacterial flagellin (FlaB) failed to elicit a NF-κB response in HCT116 cells stably expressing firefly luciferase. At least two possible differences may account for this discrepancy. First, HCT116 cell lines are not all isogenic. However, in our experiments, we utilized two different HCT116 cell lines stably carrying different NF-κB reporter constructs and both responded concordantly. Also, the TLR5 stimulus was different. We used either heat-killed *Salmonella* or flagellin derived from *Salmonella* as a TLR5 stimulus, whereas the other study (15) used flagellin derived from *Vibrio vulnificus*.

HCT116 cells have previously been shown to express TLR5, but not TLR2 and TLR4 (51), suggesting an important distinguishing attribute of this system. TLR2 and TLR4 have been shown to be predominantly pro-tumorigenic compared to the noted anti-tumorigenic properties of the flagellin-TLR5 pathway (52-55). Furthermore, TLR5 is the only known TLR family member to bind flagellin. Therefore, with HCT116 cells, we were able to utilize a *siRNA* high-throughput screen to isolate the contribution of individual host kinases to the regulation of TLR5-mediated NF-κB signaling specifically in response to bacterial flagellin.

Multiple kinases linked to the NF-κB signaling pathway were identified as modulators of TLR5-induced reporter activity in the screen. Notably, IRAK1, a kinase central to TLR signal transduction, was revealed in the screen as a positive regulator at 45 minutes and this correlated with its known role in IKK activation (56). At 245 minutes, AKT was identified by the screen as

a positive regulator of NF-κB, and indeed, AKT has been shown to contribute to full NF-κB activation and to promote nuclear NF-κB transactivation (57,58). Although *siRNA*-mediated knockdown of both MAP2K2 and MAP2K3 gave reproducible modulation of NF-κB in our screen, targeting known downstream MAP kinases with chemical inhibitors showed no consistent effect in this system. This could be explained by a model wherein the identified kinases act on other downstream proteins, as opposed to their typical MAP kinase targets, in the context of flagellin-induced signaling. Recent work identified MAP kinases as important modulators of NF-κB-induced cytokine production in intestinal epithelial cells with constitutively active NF-κB, further supporting our observation (59). Because intestinal cancers often display high levels of active NF-κB, MAPK activation in these cells may be required for full inflammatory-mediated NF-κB transcriptional activation (60). Perhaps this effect is the underlying reason for the seemingly important contribution of MAP2K2 and MAP2K3 to TLR5-induced signaling in HCT116 colon carcinoma cells seen herein. In this regard, it has been recently reported that TLRs represent upstream effectors of a nucleotide receptor signaling network, specifically, one lying upstream of MAP kinase Erk1/2 activation (26).

Despite the above confirmation hits, numerous other kinases with expected functions in the NF-κB pathway did not appear as hits in our high-throughput screen. In these instances, such as IKKβ, there are several possible reasons for lack of detection. First and foremost, such kinases may be more specific to other modes of NF-κB signaling not relevant to *Salmonella*-induced signaling. Second, as has been established with published screens (e.g., (61)), not all physiologically important kinases necessarily appear as high-stringency hits, revealing the complexity of systems and their regulation. Third, the specific kinase may be expressed at high levels or possess such a long half-life that *siRNA* knockdown was inadequate to reduce protein

levels sufficiently to affect signaling. And alternatively, for parallel pathways, host cells may have compensating co-lateral mechanisms to cope with loss of one kinase, thus preventing any phenotypic change.

Herein, targeted *siRNA* sequences against the nucleotide diphosphate kinase *NME3* had a dramatic effect on down-regulating TLR5-induced NF-κB reporter activation. *NME3* is one of eight human nucleotide diphosphate kinase genes (44). These genes are capable of utilizing ATP to form non-ATP NTPs through their catalytic kinase domain, but also have been attributed with a variety of potential functions from apoptosis regulation to cell migration to transcriptional activation (62). Two homologues of *NME3*, *NME1* and *NME2*, have been studied in more detail *(62)*. NME2 has demonstrated transcriptional activation of *cMyc*, a prominent oncogene (63). *NME3* shows about 65% homology with *NME2*, and has an additional 17 amino acid N-terminal tail (62,64). NME3 has also been shown to modulate adhesion characteristics and activate integrin expression, a known downstream target of NF-κB (42). Perhaps, like NME2, NME3 acts as a transcriptional co-regulator, and potentiates the action of NF-κB, thereby molding a pro-inflammatory transcriptional profile. In this case, NME3 may be participating in an alternative signaling pathway initiated by TLR5-induced activation of NF-κB signaling to intensify downstream cytokine release and enhance immune cell recruitment into the tumor microenvironment. Future DNA-binding studies and transcriptional profiling may help clarify whether NME3 binds DNA to help co-activate transcription, similar to its homolog, NME2.

Our data suggest that the role of NME3 in TLR5-induced NF-κB signaling may be to bolster tumor suppressive pro-inflammatory NF-κB signaling. This hypothesis is in line with previous tumor-suppressive observations in which NME3 overexpression halted differentiation and induced apoptosis within a myeloid precursor line (45), inhibited cell motility in a breast cancer

cell line (43), and inhibited proliferation *in vitro* and *in vivo* within a colorectal cancer line (50). Whereas NME3 overexpression showed tumor suppressive effects, reduced NME3 levels correlated with higher Dukes stage, poorer differentiation grade, and positive lymph node metastases in colorectal cancer patients (65). Additionally, we identified that high *NME3* expression correlated with enhanced patient survival in breast and lung cancers. Similarly, high *TLR5* expression correlated with enhanced survival for breast, lung and ovarian cancer patients, but with poorer survival for gastric cancer patients. Interestingly, TLR5 signaling has been reported to show anti-tumor activity in breast cancer (66), but promote gastric cancer cell proliferation (67). NME3-mediated enhancement of TLR5 signaling may augment tumor suppressive roles in breast, lung and ovarian cancers, but not in gastric cancer. This is further supported by the significant association between *NME3* and *TLR5* expression profiles in these cancer patients. Complementary to these results, over-expression of *CDK6*, a negative regulator of flagellin-induced NF-κB signaling (Table 1), correlated with poorer survival in breast, lung and ovarian cancer patients, but in contrast, trended toward increased survival in gastric cancer while showing no overall statistically significant effect (Fig. S7a-d). As a negative regulator of NF-κB signaling in this context, these data further support *CDK6* as a *bona fide* drug target and imply that negative regulators such as *CDK6* could be targeted to enhance flagellin-induced NF-κB signaling. Indeed, a CDK4/6 inhibitor has been recently approved by the FDA for treatment of breast cancer (41). Given that NF-κB is a downstream effector of TLR5 signaling, it is not surprising that *NF-κB1* expression was significantly associated with *NME3* and *TLR5* expression profiles in breast, lung, ovarian and gastric cancer patients. However, the finding that high *NF-κB1* expression only correlated with enhanced survival for breast cancer patients may reflect the context-dependent differences in *NF-κB1* signaling inputs between these cancers. Alternatively,

but not mutually exclusively, differences in mutational landscape amongst these cancers may contribute to these differences. Furthermore, six NME3 missense mutations were identified in various cancer types predicted to have a high impact on protein function (68,69). Five of these mutations reside within or adjacent to the predicted active site of NME3 based on conserved NME1 and NME2 active site domains (Fig. S8a,b) (70). Collectively, our data and past studies indicate that NME3 is a putative tumor suppressor and may evoke these functions via enhancement of NF-κB signaling downstream of TLR5 activation.

In summary, these results shed light on the downstream signaling mechanisms that govern the recently characterized anti-tumor effects of flagellin-mediated TLR5 signaling. For this work, we utilized HCT116, a cell line whose NF-κB pathway specifically responds to flagellin and not other bacterial components, such as LPS, peptidoglycan and NOD ligands, which negates the contribution of other TLR signaling components to our system. A live cell high-throughput screen to identify individual candidate kinases mediating the tumor cell-autonomous anti-tumor effects of flagellin identified several kinases not previously recognized, in particular, NME3. Future studies will further determine the mechanisms of how NME3 reinforces the anti-tumor activity of the TLR5-induced NF-κB pathway in tumor cells and provide insight to optimize cancer immunotherapy.

Acknowledgements

This study was supported by the National Institutes of Health grant P50 CA94056 to the Washington University-MD Anderson Cancer Center Inter-institutional Molecular Imaging Center, the Gerald Dewey Dodd, Jr., Endowed Distinguished Chair of the University of Texas MD Anderson Cancer Center, and a faculty UT STARs Award. The HTC of Washington University obtains support from the Siteman Cancer Center, supported in part by a NCI Cancer Center Support Grant (P30 CA91842), and the Biostatistics Resource of MDACC obtains support from a NCI Cancer Center Support Grant (P30 CA016672).

References

1. Leach DR, Krummel MF, Allison JP. Enhancement of antitumor immunity by CTLA-4 blockade. Science 1996;271(5256):1734-6.
2. Pardoll DM. The blockade of immune checkpoints in cancer immunotherapy. Nat Rev Cancer 2012;12(4):252-64.
3. Sivan A, Corrales L, Hubert N, Williams JB, Aquino-Michaels K, Earley ZM, et al. Commensal Bifidobacterium promotes antitumor immunity and facilitates anti-PD-L1 efficacy. Science 2015;350(6264):1084-9.
4. Garaude J, Kent A, van Rooijen N, Blander JM. Simultaneous targeting of toll- and nod-like receptors induces effective tumor-specific immune responses. Sci Transl Med 2012;4(120):120ra16.
5. Lu H. TLR agonists for cancer immunotherapy: tipping the balance between the immune stimulatory and inhibitory effects. Frontiers Immunology 2014;5:doi: 10.3389/fimmu.2014.00083.
6. Nguyen CT, Hong SH, Sin JI, Vu HV, Jeong K, Cho KO, et al. Flagellin enhances tumor-specific CD8(+) T cell immune responses through TLR5 stimulation in a therapeutic cancer vaccine model. Vaccine 2013;31(37):3879-87.
7. Frahm M, Felgner S, Kocijancic D, Rohde M, Hensel M, Curtiss R, 3rd, et al. Efficiency of conditionally attenuated Salmonella enterica serovar Typhimurium in bacterium-mediated tumor therapy. MBio 2015;6(2).
8. Pawelek JM, Low KB, Bermudes D. Tumor-targeted Salmonella as a novel anticancer vector. Cancer Res 1997;57(20):4537-44.
9. Pawelek JM, Low KB, Bermudes D. Bacteria as tumour-targeting vectors. Lancet Oncol 2003;4(9):548-56.
10. Yu B, Yang M, Shi L, Yao Y, Jiang Q, Li X, et al. Explicit hypoxia targeting with tumor suppression by creating an "obligate" anaerobic Salmonella Typhimurium strain. Scientific reports 2012;2:436.
11. Flentie K, Kocher B, Gammon ST, Novack DV, McKinney JS, Piwnica-Worms D. A bioluminescent transposon reporter-trap identifies tumor-specific microenvironment-

induced promoters in *Salmonella* for conditional bacterial-based tumor therapy. Cancer discovery 2012;2(7):624-37.

12. Forbes NS. Engineering the perfect (bacterial) cancer therapy. Nat Rev Cancer 2010;10(11):785-94.
13. al-Ramadi BK, Fernandez-Cabezudo MJ, El-Hasasna H, Al-Salam S, Bashir G, Chouaib S. Potent anti-tumor activity of systemically-administered IL2-expressing Salmonella correlates with decreased angiogenesis and enhanced tumor apoptosis. Clin Immunol 2009;130(1):89-97.
14. Rakoff-Nahoum S, Medzhitov R. Toll-like receptors and cancer. Nature Reviews Cancer 2009;9:57-63.
15. Zheng JH, Nguyen VH, Jiang SN, Park SH, Tan W, Hong SH, et al. Two-step enhanced cancer immunotherapy with engineered *Salmonella typhimurium* secreting heterologous flagellin. Sci Transl Med 2017;9(376):eaak9537.
16. Rhee SH, Im E, Pothoulakis C. Toll-like receptor 5 engagement modulates tumor development and growth in a mouse xenograft model of human colon cancer. Gastroenterology 2008;135(2):518-28.
17. Cai Z, Sanchez A, Shi Z, Zhang T, Liu M, Zhang D. Activation of Toll-like receptor 5 on breast cancer cells by flagellin suppresses cell proliferation and tumor growth. Cancer Res 2011;71(7):2466-75.
18. Galli R, Starace D, Busa R, Angelini D, Paone A, Cesaris P, et al. TLR stimulation of prostate tumor cells induces chemokine-mediated recruitment of specific immune cell types. Journal of Immunology 2010;184(12):6658-69.
19. Sfondrini L, Rossini A, Besusso D, Merlo A, Tagliabue E, Menard S, et al. Antitumor activity of the TLR-5 ligand flagellin in mouse models of cancer. J Immunol 2006;176(11):6624-30.
20. Hayashi F, Smith KD, Ozinsky A, Hawn TR, Yi EC, Goodlett DR, et al. The innate immune response to bacterial flagellin is mediated by Toll-like receptor 5. Nature 2001;410(6832):1099-103.
21. Menendez D, Shatz M, Azzam K, Garantziotis S, Fessler MB, Resnick MA. The Toll-like receptor gene family is integrated into human DNA damage and p53 networks. PLoS genetics 2011;7(3):e1001360.

22. Shatz M, Menendez D, Resnick MA. The human TLR innate immune gene family is differentially influenced by DNA stress and p53 status in cancer cells. Cancer Res 2012;72(16):3948-57.
23. Shatz M, Shats I, Menendez D, Resnick MA. p53 amplifies Toll-like receptor 5 response in human primary and cancer cells through interaction with multiple signal transduction pathways. Oncotarget 2015;6(19):16963-80.
24. Akira S, Takeda K. Toll-like receptor signalling. Nat Rev Immunol 2004;4(7):499-511.
25. Vijay-Kumar M, Gewirtz A. Flagellin: key target of mucosal innate immunity. Mucosal Immunity 2009;2:197-205.
26. McNamara N, Gallup M, Sucher A, Maltseva I, McKemy D, Basbaum C. AsialoGM1 and TLR5 cooperate in flagellin-induced nucleotide signaling to activate Erk1/2. Am J Respir Cell Mol Biol 2006;34(6):653-60.
27. Yu Y, Zeng C, H H, Vijay-Kumar M, Neish A, Merlin D, et al. STAT signaling underlies difference between flagellin-induced and tumor necrosis factor-α-induced epithelial gene expression. Journal of Biological Chemistry 2004;279:35210-18.
28. Zeng H, Wu H, Sloane V, Jones RM, Yu Y, Lin P, et al. Flagellin/TLR5 responses in epithelia reveal intertwined activation of inflammatory and apoptotic pathways. Am J Physiol Gastrointest Liver Physiol 2006;290:G96-G108.
29. Sun J, Fegan P, Desai A, Madara J, ME H. Flagellin-induced tolerance of the toll-like receptor 5 signaling pathway in polarized intestinal epithelial cells. Am J Physiol Gastrointest Liver Physiol 2006;292:G767-G78.
30. Simone R, Floriani A, Saverino D. Stimulation of human CD4+ T lymphocytes via TLR3, TLR5 and TLR7/8 up-regulates expression of costimulatory and modulates proliferation. Open Microbiol J 2009;3:1-8.
31. Rutkowski MR, Stephen TL, Svoronos N, Allegrezza MJ, Tesone AJ, Perales-Puchalt A, et al. Microbially driven TLR5-dependent signaling governs distal malignant progression through tumor-promoting inflammation. Cancer Cell 2015;27(1):27-40.
32. Datsenko KA, Wanner BL. One-step inactivation of chromosomal genes in Escherichia coli K-12 using PCR products. Proc Natl Acad Sci U S A 2000;97(12):6640-5.

33. Moss BL, Gross S, Gammon ST, Vinjamoori A, Piwnica-Worms D. Identification of a ligand-induced transient refractory period in nuclear factor-kappaB signaling. J Biol Chem 2008;283(13):8687-98.
34. Gross S, Piwnica-Worms D. Real-time imaging of ligand-induced IKK activation in intact cells and in living mice. Nat Methods 2005;2:607-14.
35. Zhang XD, Yang XC, Chung N, Gates A, Stec E, Kunapuli P, et al. Robust statistical methods for hit selection in RNA interference high-throughput screening experiments. Pharmacogenomics 2006;7(3):299-309.
36. Gyorffy B, Lanczky A, Eklund AC, Denkert C, Budczies J, Li Q, et al. An online survival analysis tool to rapidly assess the effect of 22,277 genes on breast cancer prognosis using microarray data of 1,809 patients. Breast Cancer Res Treat 2010;123(3):725-31.
37. Gyorffy B, Surowiak P, Budczies J, Lanczky A. Online survival analysis software to assess the prognostic value of biomarkers using transcriptomic data in non-small-cell lung cancer. PLoS One 2013;8(12):e82241.
38. Gyorffy B, Lanczky A, Szallasi Z. Implementing an online tool for genome-wide validation of survival-associated biomarkers in ovarian-cancer using microarray data from 1287 patients. Endocr Relat Cancer 2012;19(2):197-208.
39. Glantz SA. Primer of Biostatistics, 2nd ed, Mcgraw-Hill, Inc, New York 1987:pp. 379.
40. Tallant T, Deb A, Kar N, Lupica J, de Veer MJ, DiDonato JA. Flagellin acting via TLR5 is the major activator of key signaling pathways leading to NF-kappa B and proinflammatory gene program activation in intestinal epithelial cells. BMC Microbiol 2004;4:33.
41. Sherr CJ, Beach D, Shapiro GI. Targeting CDK4 and CDK6: from discovery to therapy. Cancer discovery 2016;6(4):353-67.
42. Amendola R, Martinez R, Negroni A, Venturelli D, Tanno B, Calabretta B, et al. DR-nm23 gene expression in neuroblastoma cells: relationship to integrin expression, adhesion characteristics, and differentiation. J Natl Cancer Inst 1997;89(17):1300-10.
43. Carinci F, Arcelli D, Lo Muzio L, Francioso F, Valentini D, Evangelisti R, et al. Molecular classification of nodal metastasis in primary larynx squamous cell carcinoma. Transl Res 2007;150(4):233-45.

44. Venturelli D, Cesi V, Ransac S, Engelhard A, Perrotti D, Calabretta B. The nucleoside diphosphate kinase activity of DRnm23 is not required for inhibition of differentiation and induction of apoptosis in 32Dcl3 myeloid precursor cells. Exp Cell Res 2000;257(2):265-71.
45. Venturelli D, Martinez R, Melotti P, Casella I, Peschle C, Cucco C, et al. Overexpression of DR-nm23, a protein encoded by a member of the nm23 gene family, inhibits granulocyte differentiation and induces apoptosis in 32Dc13 myeloid cells. Proc Natl Acad Sci U S A 1995;92(16):7435-9.
46. Choi YJ, Im E, Chung HK, Pothoulakis C, Rhee SH. TRIF mediates Toll-like receptor 5-induced signaling in intestinal epithelial cells. J Biol Chem 2010;285(48):37570-8.
47. Ben-Neriah Y, Karin M. Inflammation meets cancer, with NF-kappaB as the matchmaker. Nat Immunol 2011;12(8):715-23.
48. Hoesel B, Schmid JA. The complexity of NF-kappaB signaling in inflammation and cancer. Molecular cancer 2013;12:86.
49. Kendellen MF, Bradford JW, Lawrence CL, Clark KS, Baldwin AS. Canonical and non-canonical NF-kappaB signaling promotes breast cancer tumor-initiating cells. Oncogene 2014;33(10):1297-305.
50. Qu L, Liang L, Su J, Yang Z. Inhibitory effect of upregulated DR-nm23 expression on invasion and metastasis in colorectal cancer. Eur J Cancer Prev 2013;22(6):512-22.
51. Zhao L, Kwon M-J, Huang S, Lee J, Fukase K, Inohara N, et al. Differential modulation of nods signaling pathways by fatty acids in human colonic epithelial HCT116 cells. Journal of Biological Chemistry 2007;282:11618-28.
52. Maeda S, Hikiba Y, Sakamoto K, Nakagawa H, Hirata Y, Havakawa Y, et al. Colon cancer-derived factors activate NF-kB in myeloid cells via TLR2 to link inflammation and tumorigenesis. Mol Med Report 2011;4(6):1083-88.
53. Oblak A, Jerala R. Toll-like receptor 4 activation in cancer progression and therapy. Clin Dev Immunol 2011.
54. Xu H, Wu Q, Dang S, Jin M, Xu J, Cheng Y, et al. Alteration of CXCR7 expression mediated by TLR4 promotes tumor cell proliferation and migration in human colorectal carcinoma. PLoS One 2011;6(12):e27399.

55. Liao S, Zhou Y, Yuan Y, Li D, Wu F, Wang Q, et al. Triggering of toll-like receptor 4 on metastatic breast cancer cells promotes avB3-mediated adhesion and invasive migration. Breast Cancer Res Treat 2011.
56. Gottipati S, Rao NL, Fung-Leung WP. IRAK1: a critical signaling mediator of innate immunity. Cell Signal 2008;20(2):269-76.
57. Madrid LV, Mayo MW, Reuther JY, Baldwin AS, Jr. Akt stimulates the transactivation potential of the RelA/p65 Subunit of NF-kappa B through utilization of the Ikappa B kinase and activation of the mitogen-activated protein kinase p38. J Biol Chem 2001;276(22):18934-40.
58. Ozes ON, Mayo LD, Gustin JA, Pfeffer SR, Pfeffer LM, Donner DB. NF-kappaB activation by tumour necrosis factor requires the Akt serine-threonine kinase. Nature 1999;401(6748):82-5.
59. Guma M, Stepniak D, Shaked H, Spehlmann ME, Shenouda S, Cheroutre H, et al. Constitutive intestinal NF-kappaB does not trigger destructive inflammation unless accompanied by MAPK activation. J Exp Med 2011;208(9):1889-900.
60. Kojima M, Morisaki T, Sasaki N, Nakano K, Mibu R, Tanaka M, et al. Increased nuclear factor-kB activation in human colorectal carcinoma and its correlation with tumor progression. Anticancer Res 2004;24(2B):675-81.
61. Naik S, Dothager RS, Marasa J, Lewis CL, Piwnica-Worms D. Vascular endothelial growth factor receptor-1 Is synthetic lethal to aberrant {beta}-catenin activation in colon cancer. Clin Cancer Res 2009;15(24):7529-37.
62. Lacombe ML, Milon L, Munier A, Mehus JG, Lambeth DO. The human Nm23/nucleoside diphosphate kinases. J Bioenerg Biomembr 2000;32(3):247-58.
63. Postel EH, Berberich SJ, Flint SJ, Ferrone CA. Human c-myc transcription factor PuF identified as nm23-H2 nucleoside diphosphate kinase, a candidate suppressor of tumor metastasis. Science 1993;261(5120):478-80.
64. Boissan M, Dabernat S, Peuchant E, Schlattner U, Lascu I, Lacombe ML. The mammalian Nm23/NDPK family: from metastasis control to cilia movement. Mol Cell Biochem 2009;329(1-2):51-62.

65. Yang T, Chen BZ, Li DF, Wang HM, Lin XS, Wei HF, et al. Reduced NM23 Protein Level Correlates With Worse Clinicopathologic Features in Colorectal Cancers: A Meta-Analysis of Pooled Data. Medicine (Baltimore) 2016;95(4):e2589.
66. Shi M, Yao Y, Han F, Li Y, Li Y. MAP1S controls breast cancer cell TLR5 signaling pathway and promotes TLR5 signaling-based tumor suppression. PLoS One 2014;9(1):e86839.
67. Song EJ, Kang MJ, Kim YS, Kim SM, Lee SE, Kim CH, et al. Flagellin promotes the proliferation of gastric cancer cells via the Toll-like receptor 5. Int J Mol Med 2011;28(1):115-9.
68. Gao J, Aksoy BA, Dogrusoz U, Dresdner G, Gross B, Sumer SO, et al. Integrative analysis of complex cancer genomics and clinical profiles using the cBioPortal. Sci Signal 2013;6(269):pl1.
69. Cerami E, Gao J, Dogrusoz U, Gross BE, Sumer SO, Aksoy BA, et al. The cBio Cancer Genomics Portal: an open platform for exploring multidimensional cancer genomics data. Cancer discovery 2012;2(5):401-4.
70. Tepper AD, Dammann H, Bominaar AA, Veron M. Investigation of the active site and the conformational stability of nucleoside diphosphate kinase by site-directed mutagenesis. J Biol Chem 1994;269(51):32175-80.

Author Manuscript Published OnlineFirst on March 9, 2018; DOI: 10.1158/1541-7786.MCR-17-0603
Author manuscripts have been peer reviewed and accepted for publication but have not yet been edited.

Tables

Table 1

Negative regulators of degradation		Positive regulators of degradation		Negative regulators of resynthesis		Positive regulators of resynthesis	
Rank	Gene target	Rank	Gene target	Rank	Gene target	Rank	Gene target
1	TYRO3	1	MAP2K3	1	CDK6	1	MAP2K2
2	TGFBR2	2	MAP2K2	2	CSNK1G2	2	PIK3CG
3	PRKAR2A	3	ITPKA	3	DMPK	3	AKT1
4	CDK5R2	4	TESK1	4	BTK	4	MAPK6
5	RPS6KA5	5	PIK3CD	5	MAPK14	5	MAP2K3
6	PIM1	6	PKN2	6	BMX	6	PCTK3
7	PDK1	7	DGUOK	7	CSNK1D	7	NME3
8	GRK5	8	ALPK2	8	CKB	8	EPHB2
9	TNK2	9	EPHA3	9	NEK1	9	TGFBR2
10	RAF1	10	KDR	10	STK32C	10	PIK3CD

Table 1 Legend: *SiRNA* knockdown screen of flagellin/TLR5-induced NF-κB signaling. Top positive and negative regulatory kinases identified in the degradation and resynthesis phases of the reporter screen.

Figure Legends

Figure 1. Real-time activation of NF-κB signaling by TLR5 using heat-killed *Salmonella typhimurium*. HCT116 cells in 96-well format transiently transfected with *pκB$_5$:IκBαFLuc* were stimulated with heat-killed *Salmonella* at t=0 and bioluminescence activity imaged every 5 minutes for 6 hours. (a) Representative images show pseudocolor-coded radiance maps superimposed on black-and-white photographs of the assay plate every 20 minutes. (b) Graphical representation of the changes in photon flux as a function of time after vehicle, TNFα, or *Salmonella* addition. Data are plotted as fold-initial. Bioluminescence photon flux (photons/sec) data represent the mean of triplicate wells. (c-e) HCT116 cells stably expressing *pκB$_5$:IκBαFLuc* were stimulated with the indicated ligand at t=0 and bioluminescence activity imaged every 5 minutes for 6 hours. Data are displayed as normalized photon flux values (fold-initial, fold-vehicle). (f) HCT116 cells stimulated with heat-killed *Salmonella* wild-type, *fliC$^-$*, *fjB$^-$*, or *fliC$^-$/fjB$^-$* double mutant strains at t=0 and bioluminescence activity imaged every 5 minutes for 6 hours. Data are displayed as normalized photon flux values (fold-initial, fold-vehicle).

Figure 2. Dosed-dependent activation of the transcriptionally-coupled *κB$_5$:IκBα-FLuc* fusion reporter by flagellin and heat-killed *Salmonella* in HCT116 colon carcinoma cells and TLR5 receptor antagonists inhibit flagellin-mediated activation of the reporter. (a,b) HCT116 cells containing the *κB$_5$:IκBαFLuc* fusion reporter were stimulated with the indicated ligand at t=0 and bioluminescence activity imaged every 5 minutes for 6 hours. Data are displayed as normalized photon flux values (fold-initial, fold-vehicle). (a) HCT116 cells containing *κB$_5$:IκBαFLuc* were treated with increasing flagellin concentrations: 10 ng/ml (n=4), 20 ng/ml (n=4), 50ng/ml (n=4), 100 ng/ml (n=5), 200 ng/ml (n=5), 10 μg/ml (n=3); TNFα 20 ng/ml (n=5). (b) HCT116 cells expressing *κB$_5$:IκBαFLuc* treated with different dilutions of heat-killed *Salmonella typhimurium*

from confluent culture grown at 37°C: 1,000 fold dilution (error bars represent range of n=2), 100-fold dilution (error bars represent range of n=2), 10-fold dilution (n=3); TNFα 20 ng/ml (n=5). (c,d) HCT116 cells containing the *κB$_5$:IκBαFLuc* fusion reporter were treated with two different hTLR5 antagonists and stimulated with the indicated ligand at t=0. Bioluminescence activity was image every 5 minutes for 6 hours. Data are displayed as normalized photon flux values (fold-initial, fold-vehicle). (c) Prior to cell stimulation with flagellin or TNFα, flagellin or TNFα were pre-incubated with or without soluble hTLR5 receptor (shTLR5, 5 μg/ml), then added to cells: TNFα 20 ng/ml (n=5), TNFα 20 ng/ml with shTLR5 5 μg/ml (n=5); flagellin 100 ng/ml (n=5), flagellin 100 ng/ml with shTLR5 5 μg/ml (n=5); flagellin 1 μg/ml (n=4), flagellin 1 μg/ml with shTLR5 5 μg/ml (n=4); shTLR5 5μg/ml alone (n=5). (d) Prior to stimulation with flagellin or TNFα, cells were pre-incubated with antibody against hTLR5 [hTLR5(Ab)] for an hour: TNFα 20 ng/ml (n=5), TNFα 20 ng/ml with hTLR5(Ab) 10 μg/ml (n=5); flagellin 100 ng/ml (n=5), flagellin 100 ng/ml with hTLR5(Ab) 10 μg/ml (n=5); flagellin 1 μg/ml (n=4), flagellin 1 μg/ml with hTLR5(Ab) 10 μg/ml (n=4); hTLR5(Ab) 10 μg/ml alone (n=5). Error bars represent S.E.M. for the indicated number of independent experiments.

Figure 3. A schematic of the high-throughput screening technique and high-throughput screening data. (a) HCT116 cells stably expressing *κB$_5$:IκBαFLuc* were plated into 96-well plates. After a 24-hour incubation, cells were transfected with *siRNA* from the library and incubated for 48 hours more. To image, cells were transferred into D-luciferin-containing media, allowed to equilibrate for 45 minutes, stimulated with heat-killed *Salmonella* and imaged for reporter activity at 0, 45 and 245 minutes. (b) Each *siRNA* library plate contained targeting *siRNA* in columns 2-11 and control *siRNA* constructs in columns 1 and 12, as indicated. Control wells included: mock-transfected cells (blue, A1), vehicle-treated wells (yellow; E1, F1, G1,

H1), three non-targeting control sequences (turquoise; Qiagen Allstar Negative control, F12, Qiagen scrambled *siRNA*, G12, Qiagen GFP *siRNA*, H12), TLR5-targetting *siRNA* sequences (red; IDT, C1, C12, D1, D12), and a firefly luciferase-targeting PGL3 *siRNA* (purple; Dharmacon Research Inc, A12, B12). (c,d) Normalized photon flux data for 691 targeted kinases are shown at 45 min (c) and 245 min (d) after *Salmonella* stimulation. Data are the average of three replicates. Dashed red and dotted blue lines show significance cut-offs for low ($\alpha = 0.1$) and high ($\alpha = 0.02$) stringency targeted error rates, respectively.

Figure 4. MAP2K2, MAP2K3 and NME3 act as positive regulators of TLR5-induced NF-κB signaling. A schematic diagram shows the proposed regulatory activity on NF-κB by kinase targets in each of four quadrants in the plot (*insert*). The normalized photon flux data from the primary screen at 45 minutes and 245 minutes are plotted on the x- and y-axes, respectively. Highlighted points show data from specific screening hits and TLR5 control wells. Blue triangle, TLR5; red squares, MAP2K3, MAP2K2, and AKT1; green diamond, NME3. The dotted blue line represents significance cut-offs for a high stringency ($\alpha = 0.02$) targeted error rate (high confidence hits).

Figure 5. NME3 regulates TLR5-induced NF-κB signaling. (a) *NME3* and *MyD88* knockdown inhibits NF-κB signaling. HCT116 cells stably expressing *κB_5:IκBαFLuc* and transfected with the indicated heterogeneous *siRNA* sequences were stimulated with heat-killed *Salmonella* and imaged for reporter activity every 5 minutes for 6 hours. Data are displayed as normalized photon flux values (fold-initial, fold-vehicle). Inserts, quantitative PCR verifies knockdown of *NME3* (top) or *MyD88* (bottom) mRNA in corresponding *siRNA*-treated HCT116 cells. (b-d) Targeting *NME3* by shRNA reduces NF-κB responsiveness. (b) HCT116 cells were subjected to lentiviral knockdown with the indicated shRNA constructs and transfected with the

pκB$_5$:IκBαFLuc plasmid. Cells were then stimulated with heat-killed *Salmonella* and imaged for reporter activity every 5 minutes for 6 hours. Data are displayed as normalized photon flux values (fold-initial, fold-vehicle). (c) HCT116 cells were subjected to lentiviral knockdown with the indicated shRNA constructs and transfected with the *pκB$_5$:FLuc* plasmid. Imaging was performed at 0, 2, 4, 6, and 7 hours following stimulation with *Salmonella.* Data are displayed as normalized photon flux values (fold-initial, fold-vehicle). Error bars represent standard deviation with propagated error. (d) Semi-quantitative PCR verifies knockdown of *NME3* mRNA in shRNA-expressing HCT116 cells. GAPDH mRNA levels are shown as a control. Primer dimers are observably cut at the bottom of the gel (right). (e) NME3 over-expression (insert) enhances NF-κB transcriptional activation. HCT116 cells stably expressing *κB5:IκBαFLuc* were transfected with the indicated plasmid constructs, stimulated with heat-killed *Salmonella* and imaged for reporter activity every 5 minutes for 6 hours. Data are displayed as normalized photon flux values (fold-initial, fold-vehicle).

Figure 6. *NME3* mRNA levels correlate with overall patient survival in various cancers. Gehan-Breslow-Wilcoxon test were used to estimate the *p*-values between high and low expression groups (using top and bottom 25% as the cutoff for grouping). (a) Kaplan-Meier survival analysis in breast cancer patients (n=3,951) indicates that high *NME3* expression correlates with longer patient survival ($p < 0.0001$). (b) Kaplan-Meier survival analysis of lung cancer patients (n=1926) indicates that high *NME3* expression correlates with longer patient survival ($p < 0.0001$). (c) Kaplan-Meier survival analysis of ovarian cancer patients (n=1435) shows overall no significant difference ($p < 0.22$) in survival between patients with higher or lower *NME3* expression levels. (d) Higher *NME3* expression in gastric cancer patients (n=876) significantly correlates ($p < 0.002$) with poorer survival.

Figure 7. *NME3* expression significantly correlates with *TLR5* expression. Pearson Chi-square tests were used to estimate the *p*-values between *NME3* and *TLR5* expression. (a) Mosaic plot in breast cancer patients (n=3,951) indicates that high *NME3* expression correlates with *TLR5* expression ($p < 0.0001$). (b) Mosaic plot in lung cancer patients (n=1,926) indicates that high *NME3* expression correlates with *TLR5* expression ($p < 0.0001$). (c) Mosaic plot in ovarian cancer patients (n=1,435) indicates that high *NME3* expression correlates with *TLR5* expression ($p < 0.0001$). (d) Mosaic plot in gastric cancer patients (n=876) indicates that high *NME3* expression correlates with *TLR5* expression ($p < 0.0001$). Blue shades indicate positive Pearson residuals (strong association); grey indicates Pearson residuals close to 0 (null); red shades indicate negative Pearson residuals (strong inverse association).

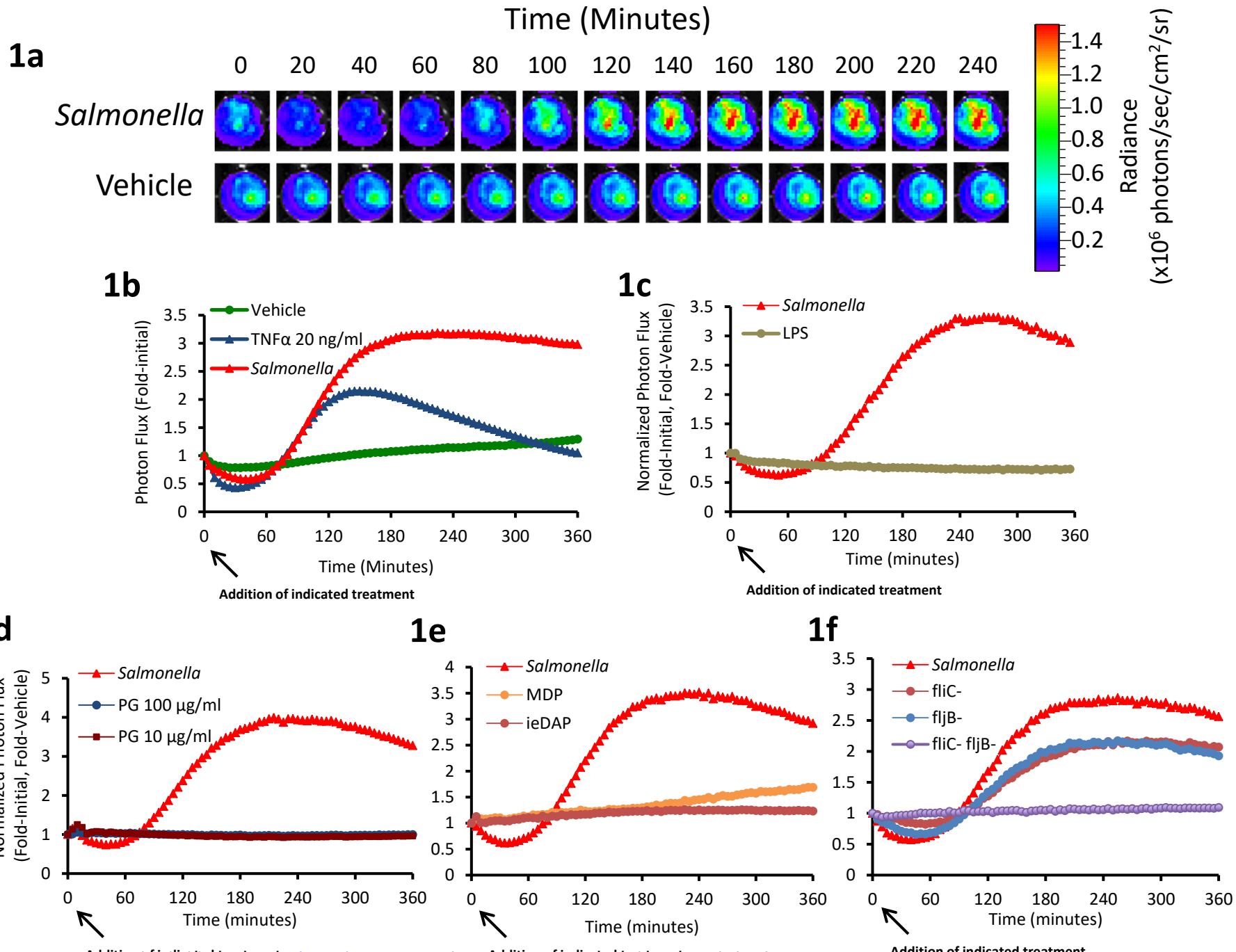

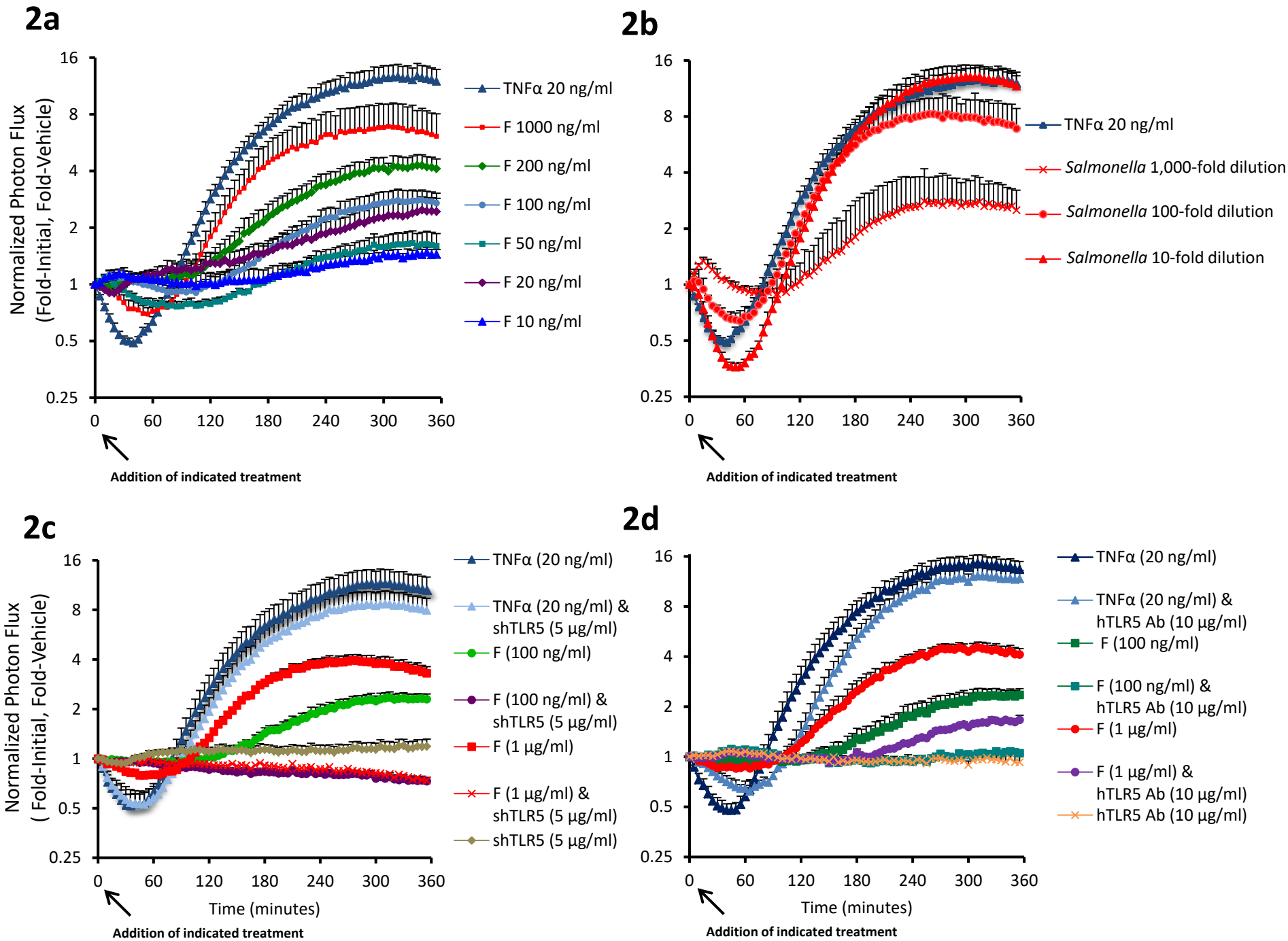

3a

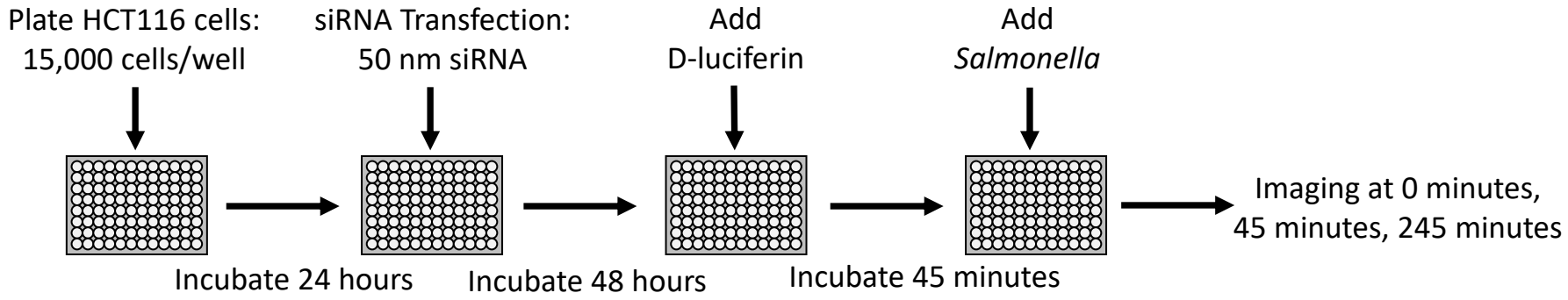

3b

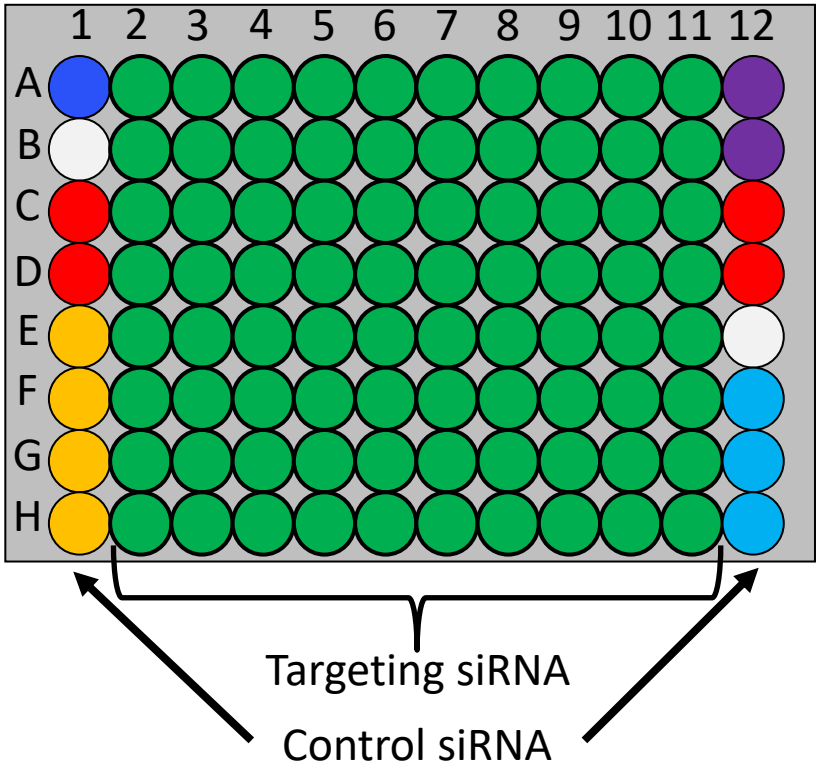

3c

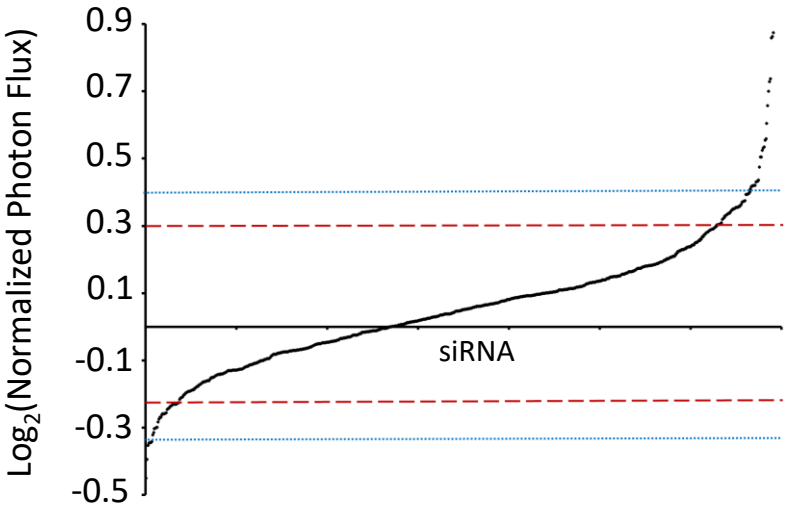

3d

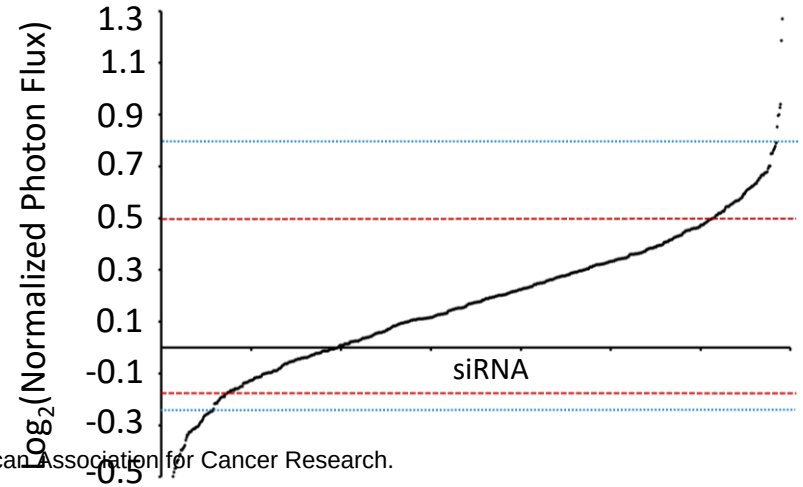

4

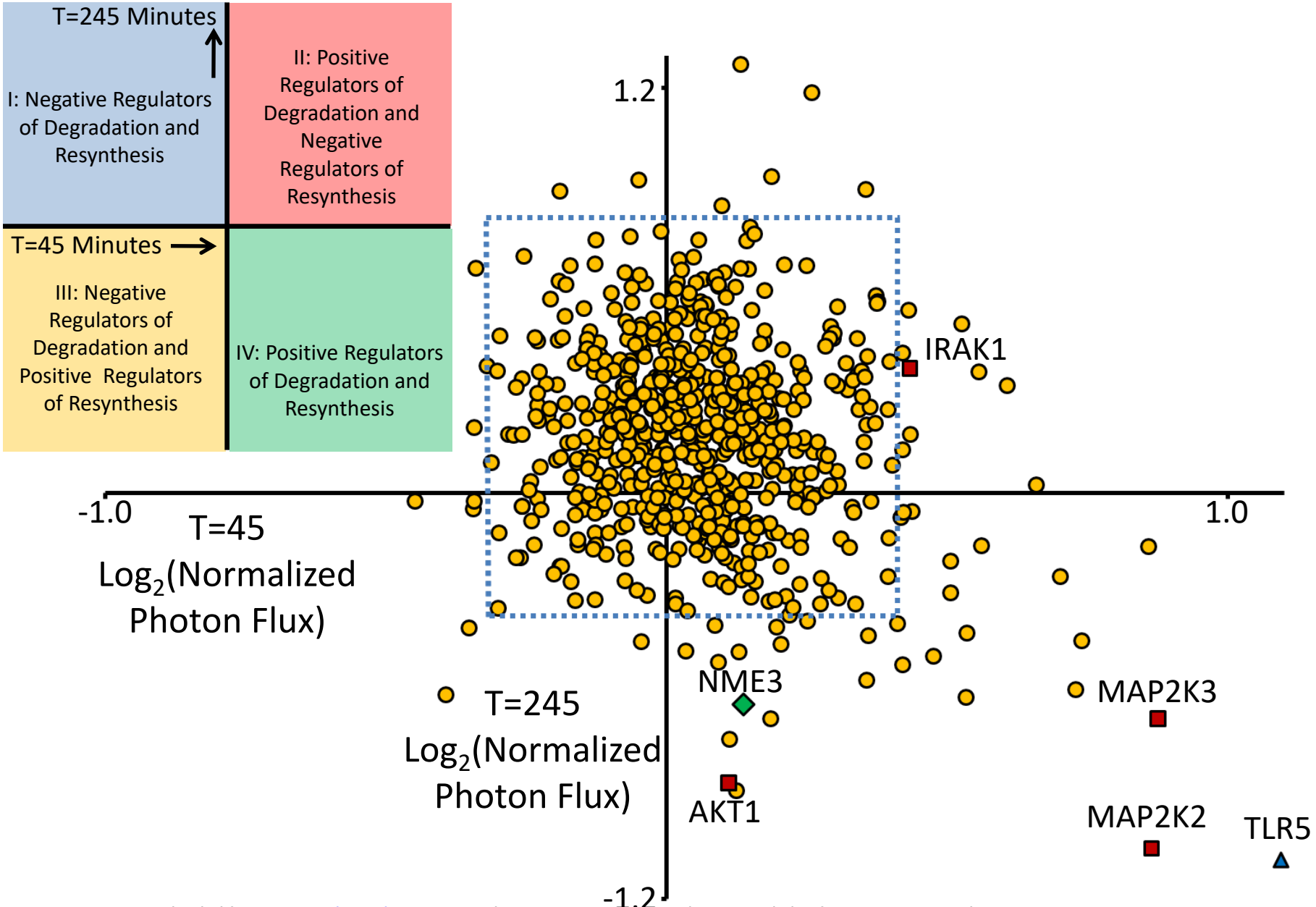

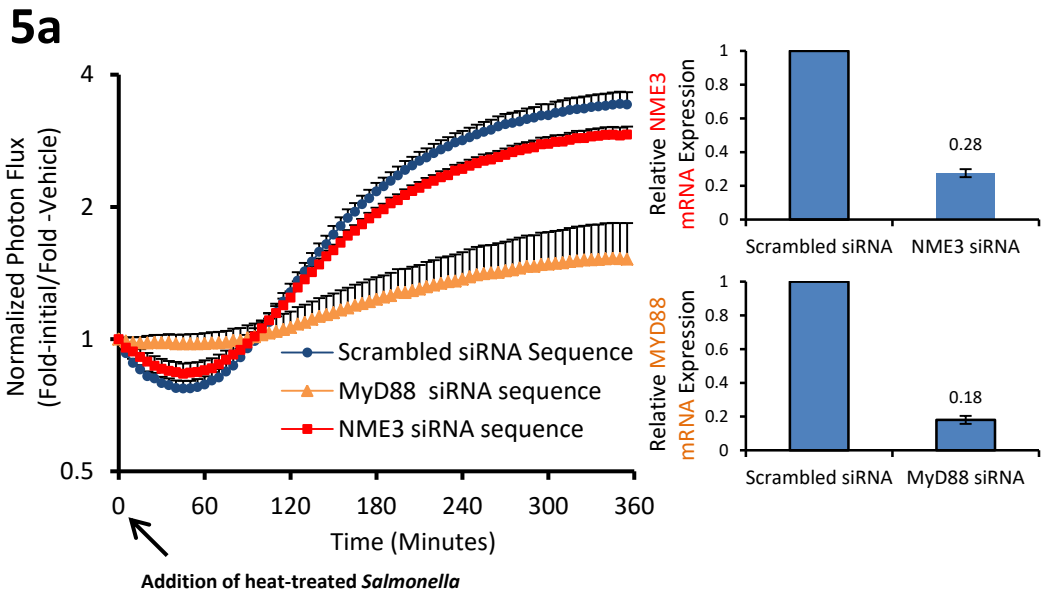

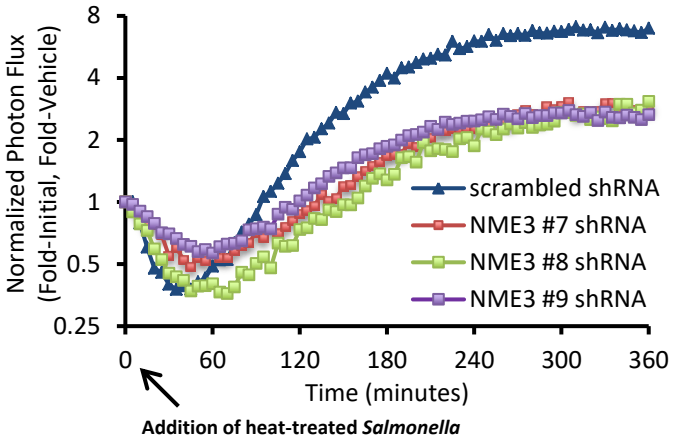

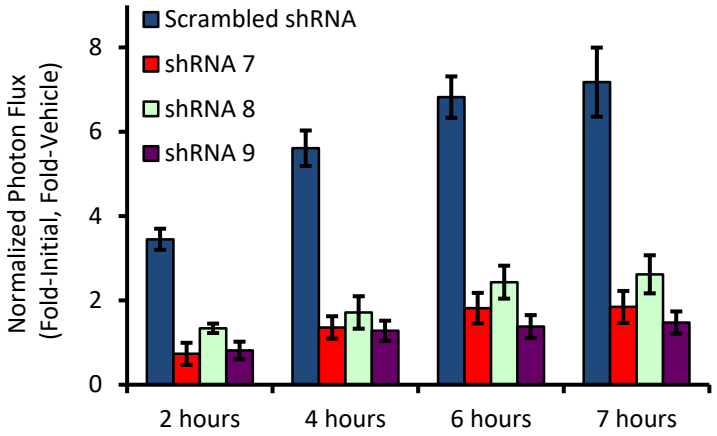

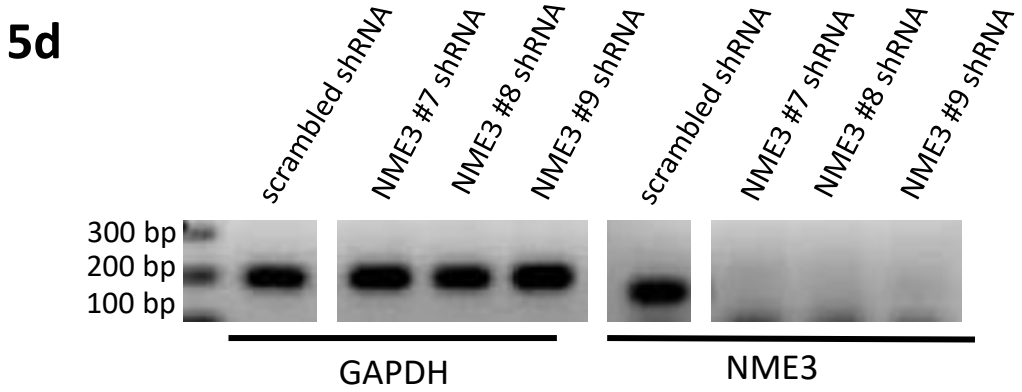

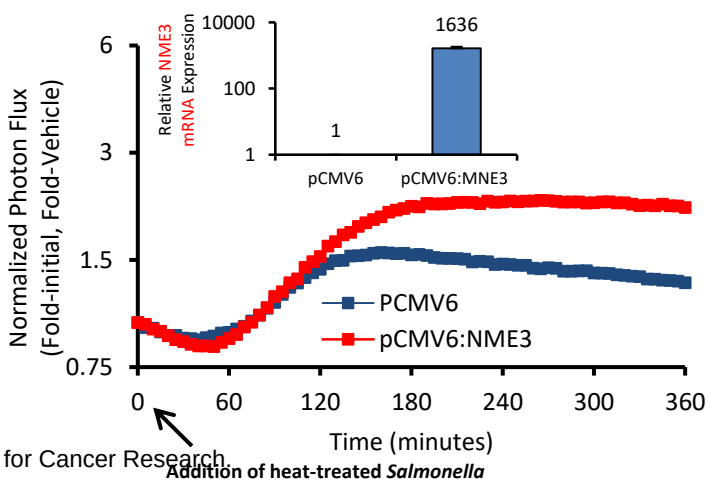

6a

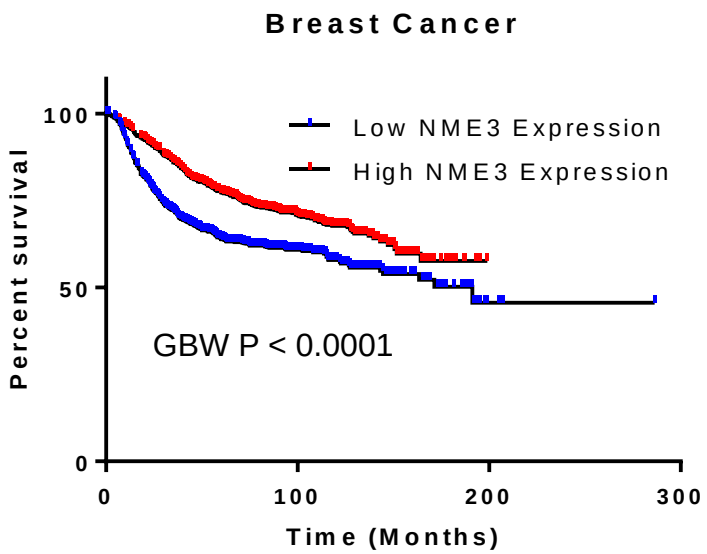

6b

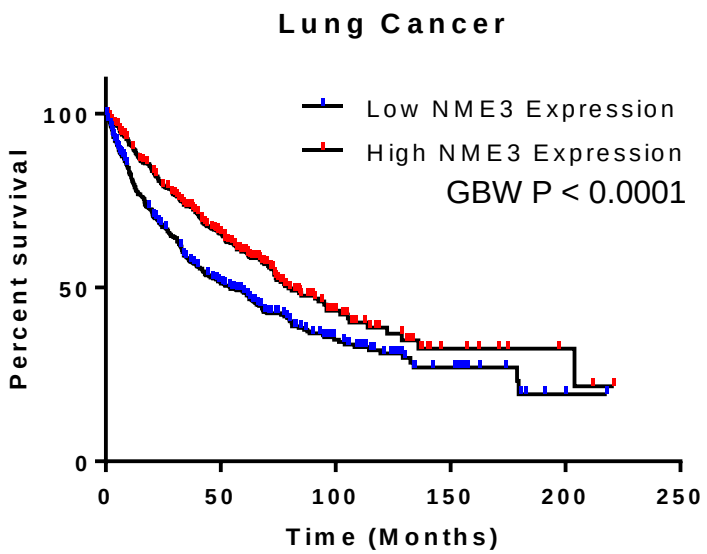

6c

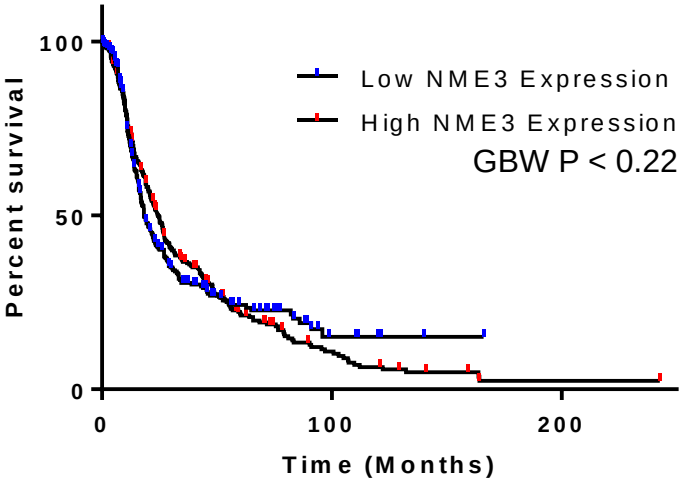

6d

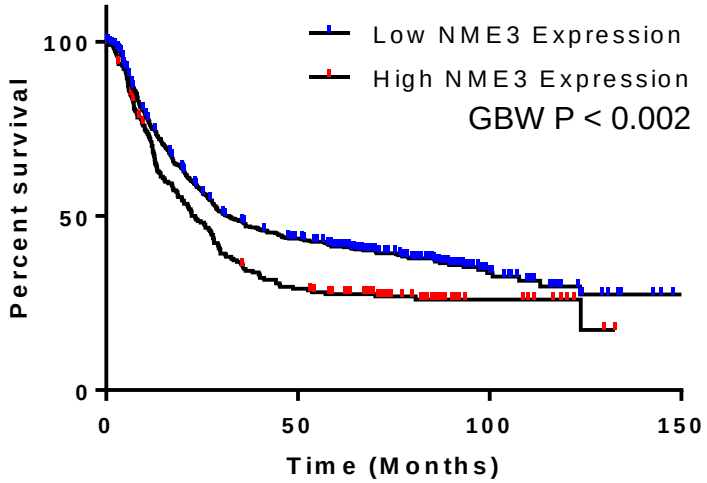

7a

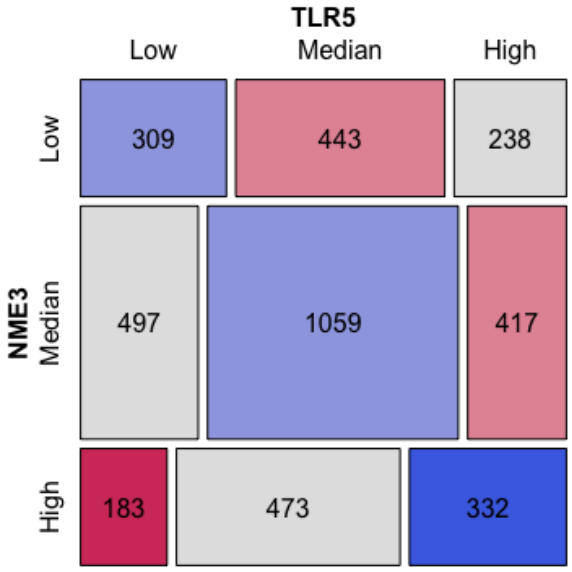

Breast Cancer

7b

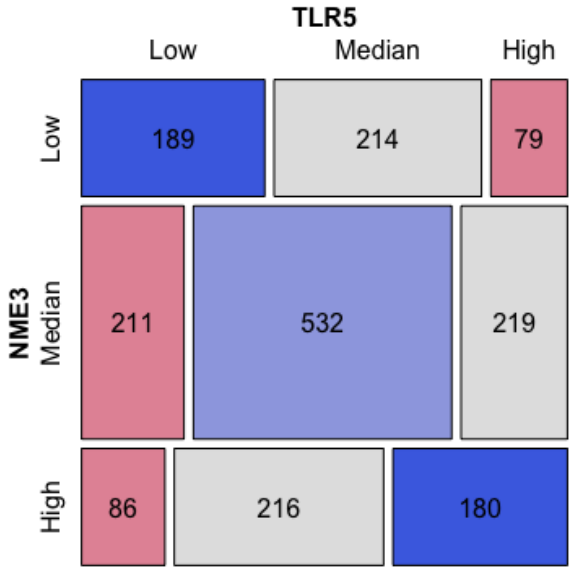

Lung Cancer

7c

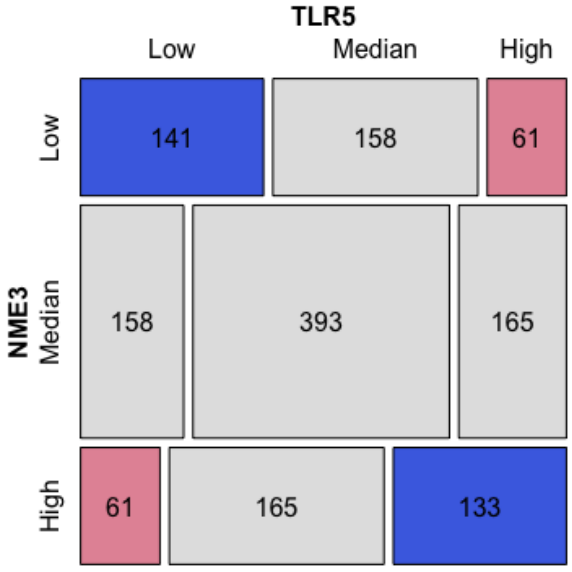

Ovarian Cancer

7d

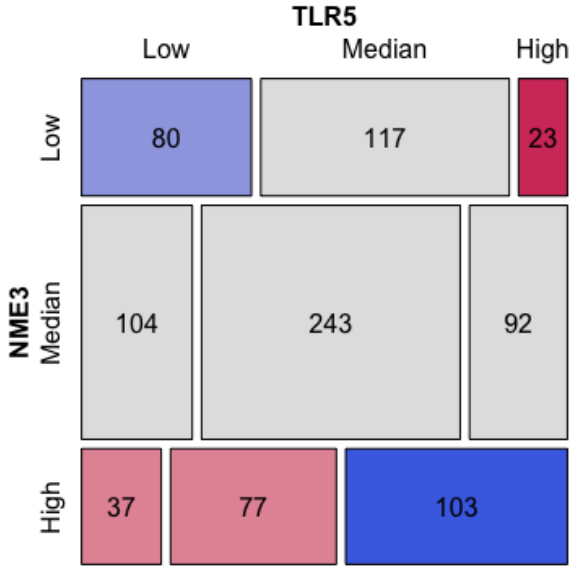

Gastric Cancer

AACR American Association for Cancer Research

Molecular Cancer Research

Nucleoside Diphosphate Kinase-3 (NME3) Enhances TLR5-Induced NF- κB Activation

Kelly Flentie, Caleb Gonzalez, Brandon Kocher, et al.

Mol Cancer Res Published OnlineFirst March 9, 2018.